

# The UV colours and dust attenuation of Lyman-break galaxies.

V. Gonzalez-Perez<sup>1,2</sup>, C. G. Lacey<sup>1</sup>, C. M. Baugh<sup>1</sup>, C. S. Frenk<sup>1</sup>, S. M. Wilkins<sup>3</sup>

<sup>1</sup>*Institute for Computational Cosmology, Department of Physics, University of Durham, South Road, Durham, DH1 3LE, U.K.*

<sup>2</sup>*Centre de Physique des Particules de Marseille, Aix-Marseille Université, CNRS/IN2P3, F-13288 Marseille cedex 9, France.*

<sup>3</sup>*University of Oxford, Department of Physics, Denys Wilkinson Building, Keble Road, OX1 3RH, U.K.*

11 September 2018

## ABSTRACT

Using GALFORM, a semi-analytical model of galaxy formation in the  $\Lambda$  cold dark matter cosmology, we study the rest-frame ultraviolet (UV) colours of Lyman-break galaxies (LBGs) in the redshift range  $2.5 \leq z \leq 10$ . As the impact of dust on UV luminosity can be dramatic, our model includes a self-consistent computation of dust attenuation based on a radiative transfer model. We find that intrinsically brighter galaxies suffer stronger dust attenuation than fainter ones, though the relation has a large scatter. The model predicts galaxies with UV colours consistent with the colour selection regions designed to select LBGs in observational surveys. We find that the drop-out technique that selects LBGs based on two rest-frame UV colours is robust and effective, selecting more than 70 per cent of UV bright galaxies at a given redshift. We investigate the impact on the predicted UV colours of varying selected model parameters. We find that the UV colours are most sensitive to the modelling of dust attenuation and, in particular, to the extinction curve used in the radiative transfer calculation. If we assume a Milky Way dust extinction curve, the predicted UV continuum slopes are, in general, bluer than observed. However, we find that the opposite is true when using the Small Magellanic Cloud dust extinction curve. This demonstrates the strong dependence of UV colours on dust properties and highlights the inadequacy of using the UV continuum slope as a tracer of dust attenuation without any further knowledge of the galaxy inclination or dust characteristics in high redshift galaxies.

**Key words:** galaxies: evolution, galaxies: formation, galaxies: high-redshift.

## 1 INTRODUCTION

The recent availability of near infrared (IR) imaging on the Wide Field Camera 3 (WFC3) on board the Hubble Space Telescope (HST), extending the wavelength coverage to span 2000Å to 17000Å, has dramatically increased the number of candidate high redshift galaxies with  $z > 2.5$  (e.g. Hathi et al. 2010; Oesch et al. 2010; Wilkins et al. 2011a,b; McLure et al. 2011; Bouwens et al. 2012). The galaxy redshift “record” has been tentatively pushed up to  $z = 10$ , with 3 candidates awaiting spectroscopic confirmation (Yan et al. 2010; Bouwens et al. 2011).

Lyman-break galaxies are selected by targeting spectral features of star-forming galaxies at  $z \geq 2.5$ , in particular the Lyman break, a combination of both the Lyman-limit break (at 912Å) due to neutral hydrogen in each galaxy and the Lyman- $\alpha$ -break (at 1216Å) due to absorption by intervening neutral gas clouds, and the UV continuum slope. Steidel et al. (1996) proved the usefulness of this technique by spectroscopically confirming drop-out candidates

isolated photometrically at  $z \sim 3$ . Since then, this approach has been adapted to find higher redshift galaxies using both ground and space based telescopes (Steidel et al. 1999; Bouwens et al. 2003; Shimasaku et al. 2005; Yoshida et al. 2006).

At these high redshifts, we are witnessing the rapid evolution of very young galaxies, when the Universe was less than a quarter of its current age. Studies of galaxies selected using the drop-out technique have been fundamental in unveiling the global star formation history of the Universe (Madau et al. 1996; Steidel et al. 1999). Moreover, observations at redshifts above  $z = 6$  could help us to understand the end of the reionisation of the intergalactic medium (e.g. Robertson et al. 2010). However, the interpretation of the observational data is likely to be significantly affected by the attenuation of starlight due to dust (e.g. Chapman et al. 2005).

Currently, there is some controversy over the level of dust attenuation inferred in LBGs. McLure et al. (2011) and Finkelstein et al. (2011) estimated the far UV attenuation

using spectral energy distribution (SED) fitting for LBGs brighter than  $M_{AB}(1500\text{\AA}) - 5\log h = -17$ . Both studies used template spectra including dust attenuation following the Calzetti law. Finkelstein et al. inferred an attenuation at  $1500\text{\AA}$ ,  $A_{1500}$ , of  $\sim 1.3$  magnitudes at  $z \sim 4$  and  $A_{1500} < 0.25$  at  $z \sim 7$ . In contrast, for galaxies with  $\langle z \rangle = 6.5$ , McLure et al. found  $\langle A_{1500} \rangle \sim 0.4$ , a value above the upper limit found by Finkelstein et al. In many observational studies the dust attenuation is inferred from the UV continuum slope estimated from a single colour. Bouwens et al. (2011) measured an average UV continuum slope of  $-3$  for galaxies at  $z = 7$ . However, this value was measured to be  $\sim -2.2$  when more data were collected by the HST WFC3 (Bouwens et al. 2012). This illustrates how the scarcity of high redshift data can bias the estimation of dust attenuation.

Dust can absorb and scatter photons either into or out of the line of sight to the observer. The outcome of these processes depends strongly on the geometry of dust and stars in galaxies and a full radiative transfer model is required for a realistic calculation of the effect of dust on star light (Fontanot et al. 2009; Fontanot & Somerville 2011). Observationally, the attenuation by dust of the UV light emitted by LBGs is usually estimated from the observed UV continuum slope (Meurer et al. 1999). Calzetti et al. (2000) proposed a universal shape for the dependence of the attenuation on wavelength, such that the UV light is the most affected by dust. This so called ‘‘Calzetti law’’ is based on observations of 39 nearby UV-bright starburst galaxies. However, the Calzetti law provides a poor fit to the UV colours of larger samples of nearby galaxies that have a range of star formation rates (Conroy et al. 2010; Buat et al. 2011b; Wild et al. 2011). Other observational studies also find that, at least for part of the UV-selected galaxies at  $1 < z < 4$ , the attenuation is not well described by the Calzetti law (Noll et al. 2009; Buat et al. 2011a, 2012; Reddy et al. 2012; Lee et al. 2012).

In this paper we use a semi-analytical approach to model the formation and evolution of galaxies with a realistic treatment of dust. In particular, we study the rest-frame UV colours of LBGs within a cold dark matter universe using GALFORM, the semi-analytical model developed initially by Cole et al. (2000).

Previous theoretical studies of LBGs include both semi-analytical (Baugh et al. 1998; Guo & White 2009; Lo Faro et al. 2009; Lacey et al. 2011; Somerville et al. 2012) and gas-dynamical simulations of galaxy formation (Nagamine 2002; Finlator et al. 2006; Forero-Romero et al. 2010; Cen 2011; Jaacks et al. 2012; Dayal & Ferrara 2012). This latter type of simulation has the drawback that, on the whole, they do not predict a present-day galaxy population consistent with observations, unlike the semi-analytical models. Furthermore, most of these models treat the attenuation by dust by using either the Calzetti law or the slab model. Guo & White (2009), Lo Faro et al. (2009) and Somerville et al. (2012) investigated the effects on the inferred luminosity functions and other properties of applying observational LBG colour selections to model galaxies. Guo & White used a phenomenological model for dust attenuation, while Lo Faro et al. used a physical model similar to that in the present paper, but restricted their analysis to LBGs at  $4 \leq z \leq 6$ . Somerville et al. studied galax-

ies at  $0 \leq z \leq 5$ , calculating the dust attenuation using a slab model with two dust components, diffuse and molecular clouds. They found that in order to reproduce the observations, they needed to let the effective optical depth normalisation evolve with redshift.

In this study, we use the version of GALFORM developed by Baugh et al. (2005) model, but with the theoretical treatment of dust attenuation described in Lacey et al. (2011), in place of the GRASIL (Silva et al. 1998) model, which was used in the original paper. GRASIL is a spectrophotometric code which is quite expensive computationally and, thus, difficult to run for large samples of galaxies. The parameters of the Baugh et al. (2005) model were set in order to match observations of sub-mm selected galaxies, with a median redshift  $z \sim 2$ , and the LBG luminosity function at  $z \sim 3$  within a single framework, at the same time as reproducing the properties of local galaxies. Lacey et al. (2011) found that the Baugh et al. model predicts UV luminosity functions that agree with observations up to  $z = 10$ , the highest redshift for which measurements are currently available. This agreement is notable as most of these observations were not available at the time the model was proposed. A typical attenuation in the UV of about two magnitudes was predicted for bright galaxies, posing the questions of whether or not a model with such strong attenuation requires galaxies with unrealistic dust contents, and if it could produce UV colours consistent with those observed.

Here, we show that the Baugh et al. model produces galaxies with the right colours to be selected as LBGs over the redshift interval  $3 \leq z \leq 10$ . We also investigate the attenuation by dust in the model. Intrinsically bright galaxies are predicted to be heavily extinguished in the model. Nevertheless, the UV continuum slope inferred from the attenuated photometry of model galaxies is *not* necessarily redder than observed. In fact, our calculations show that the UV continuum slope is a poor indicator of dust attenuation, as our results are extremely sensitive to the choice of extinction curve used as the input to the attenuation of starlight calculations. For our standard choice, a Milky Way (MW) extinction curve, galaxies get *bluer* when they are attenuated, which, as we explain in Section §6 is due to the presence of a bump at  $2175\text{\AA}$  in the extinction curve. The discrepancy between the model predictions and the observations for the slope of the attenuated UV continuum slope is smaller than the difference in the predictions on replacing the MW extinction curve by an SMC-like extinction curve.

In section §2 we summarise the main features of the Baugh et al. (2005) model. The drop-out technique is introduced in section §3. Section §4 presents the predicted dust masses and attenuation in the UV for bright galaxies at different redshifts. In sections §5 and §6 we explore the predicted UV colours and UV continuum slope for galaxies with  $z > 2.5$ . The conclusions may be found in §7.

All the magnitudes quoted are on the AB system, unless stated otherwise.

## 2 GALAXY FORMATION MODEL

We predict the UV luminosities and colours of galaxies in a  $\Lambda$  Cold Dark Matter ( $\Lambda$ CDM) universe using the GALFORM semi-analytical galaxy formation model initially de-

veloped by Cole et al. (2000). Semi-analytical models use simple, physically motivated equations to follow the fate of baryons in a universe in which structure grows hierarchically through gravitational instability (see Baugh 2006; Benson 2010, for an overview of hierarchical galaxy formation models).

GALFORM models the main processes which shape the formation and evolution of galaxies. These include: (i) the collapse and merging of dark matter haloes; (ii) the shock-heating and radiative cooling of gas inside dark matter haloes, leading to the formation of galaxy discs; (iii) quiescent star formation in galaxy discs; (iv) feedback from supernovae (SNe) and from photoionization of the intergalactic medium (IGM); (v) chemical enrichment of the stars and gas; (vi) galaxy mergers driven by dynamical friction within common dark matter haloes, leading to the formation of stellar spheroids, which also may trigger bursts of star formation. The end product of the calculations is a prediction for the number and properties of galaxies that reside within dark matter haloes of different masses.

We focus our attention on the Baugh et al. (2005) model. Some of the key features of this model are (i) a time-scale for quiescent star formation that varies simply as a power of the disc circular velocity (see Lagos et al. 2011, for a study of different star formation laws in quiescent galaxies), (ii) bursts of star formation are triggered only by galaxy mergers, (iii) a Kennicutt (1983) initial mass function (IMF) is adopted in quiescent star formation in galactic discs, while in starbursts a top-heavy IMF is assumed, with slope  $x = 0$ , (iv) the inclusion of SNe feedback with the possible occurrence of superwinds (see Benson et al. 2003, for a discussion of the effect that feedback has on the luminosity function of galaxies), and (v) feedback from the ionisation of the IGM is approximated by a simple model in which gas cooling is completely suppressed in haloes with circular velocities less than  $30 \text{ km s}^{-1}$  at redshifts  $z < 10$  (Lacey et al. 2011). In sections §2.1 and §2.2, we give a detailed account of how the attenuation due to dust and the IGM are implemented in this model. The parameters of this model were fixed with reference to a subset of the available observations of galaxies, mostly at low redshift. The Baugh et al. model uses the canonical ( $\Lambda$ CDM) parameters: matter density,  $\Omega_0 = 0.3$ , cosmological constant,  $\Lambda_0 = 0.7$ , baryon density,  $\Omega_b = 0.04$ , a normalisation of density fluctuations given by  $\sigma_8 = 0.93$  and a Hubble constant today of  $H_0 = 100h \text{ km s}^{-1} \text{ Mpc}^{-1}$ , with  $h = 0.7$ . The model employs merger trees generated using a Monte Carlo algorithm. Here we use the algorithm introduced by Parkinson et al. (2008). González et al. (2011) reported that using this particular approach does not change any of the original model predictions. We refer the reader to Baugh et al. (2005), Lacey et al. (2008) and Lacey et al. (2011) for a full description of this model.

In addition to reproducing local galaxy data, the Baugh et al. model matches the number and redshift distribution of galaxies detected by their emission at sub-millimetre wavelengths (Baugh et al. 2005; Lacey et al. 2008), the rest-frame UV luminosity function of Lyman-break galaxies up to  $z \sim 10$  (Lacey et al. 2011) and the abundance and clustering of Lyman- $\alpha$  emitters (Orsi et al. 2008). Raičević et al. (2011) used the Baugh et al. model to explore the emissivity of ionising photons at  $z \geq 6$ . González et al. (2012) showed that the Baugh et al. model

predicts that most present day galaxies with masses close to that of the MW had a LBG progenitor at  $3 < z < 4$ .

No parameters have been tuned for the study presented here. We do vary some of the parameters in the model in §5 and §6 to illustrate the sensitivity of the model predictions to our choices.

## 2.1 Dust attenuation

Following the approach presented in Cole et al. (2000) and Lacey et al. (2011, 2012), the attenuation of starlight by dust is modelled in a physically self-consistent way, based on the results of a radiative transfer calculation for a realistic geometry in which stars are distributed in a disk plus bulge. This geometry is the same as that assumed in more detailed computations carried out in the GRASIL code (Silva et al. 1998). An important feature of the method is that the dust attenuation varies self-consistently with other galaxy properties such as size, gas mass, and metallicity.

Dust can absorb photons and scatter them either into or out of the line of sight to the observer. Here we refer to dust “attenuation” as the average effect that dust has on starlight once the geometric configuration of dust and stars is taken into account. Dust attenuation includes the effects of both light absorption and scattering, which strongly depend on how dust is distributed with respect to the stars in a galaxy. We can express the dust attenuation,  $a_\lambda$ , as the ratio between the attenuated and unattenuated luminosity of a galaxy:

$$a_\lambda = \frac{L_\lambda(\text{attenuated by dust})}{L_\lambda(\text{unattenuated by dust})}. \quad (1)$$

The effective optical depth at a given wavelength can be related directly to the dust attenuation at that wavelength:  $\tau_{\text{eff}, \lambda} = -\ln(a_\lambda)$ . We can also express the attenuation in terms of magnitudes,  $A_\lambda$ , and then  $\tau_{\text{eff}, \lambda} = A_\lambda / (2.5 \log e)^1$ .

Usually the term dust “extinction” refers to the attenuation of the light from a point source placed behind a screen of dust. Thus, the “extinction” is independent of the geometry of the system.

In GALFORM, dust is assumed to be in two components: dense molecular clouds embedded in a diffuse component. Stars inside molecular clouds have their light attenuated both by the clouds and by the diffuse medium, while the remaining stars are attenuated only by the diffuse medium.

### 2.1.1 Diffuse component

The attenuation of starlight by the diffuse component of dust is calculated using the radiative transfer models of Ferrara et al. (1999). These models assume that stars are distributed in two components: an exponential disk and a bulge; and that dust is smoothly distributed in the same plane as the stellar disk. Given an extinction law, by default the MW one, the Ferrara et al. (1999) models give dust attenuation factors separately for the disc and spheroid light, as a function of wavelength, galaxy inclination, ratio of bulge

<sup>1</sup> Throughout all the paper we use the notation  $\log$  to designate the logarithm in base 10.

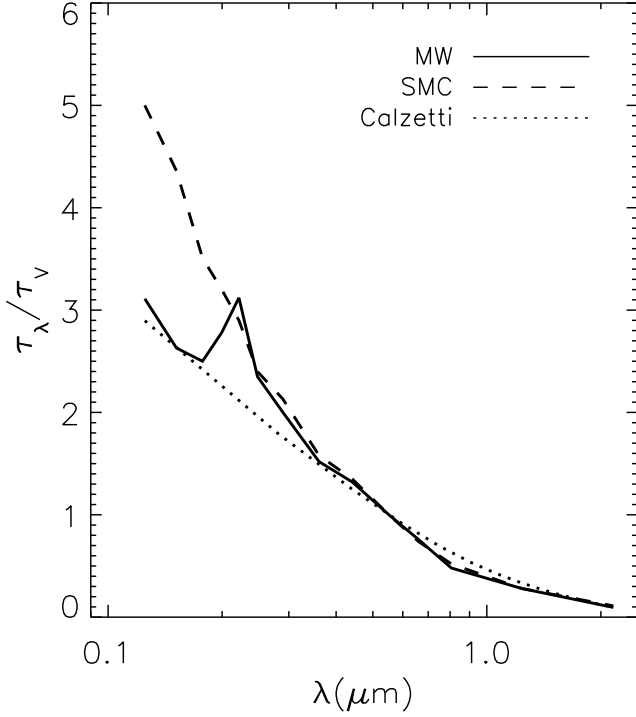


**Figure 1.** The optical depth normalised by its value in the V-band as a function of wavelength. We plot the extinction curves from the MW (solid line) and SMC (dashed line) used by Ferrara et al. (1999) to estimate the attenuation curves of galaxies, and the attenuation curve proposed by Calzetti et al. (2000) to describe observations of nearby star forming galaxies (dotted line).

to disc radial dust scalelength,  $r_e/h_R$ , ratio of dust to stellar vertical scaleheights,  $h_{z,dust}/h_{z,stars}$ , and  $\tau_{V_0}$ . Here  $\tau_{V_0}$  is the extinction optical depth in the V-band looking through the centre of a face-on galaxy. In GALFORM, the diffuse component of dust is assumed to follow the distribution of stars in a disk or in a starburst component. By default, the dust is assumed to have the same radial and vertical scalelengths as the stars. The rest of the above properties are predicted by GALFORM.

In order to calculate the extinction optical depth in the V-band,  $\tau_{V_0}$ , the extinction  $A_V$  along the line-of-sight is determined from the neutral hydrogen column density,  $N_H$ , and the cold gas metallicity,  $Z_{\text{cold}}$ :

$$A_V = \left( \frac{N_H}{\text{cm}^{-2}} \right) \left( \frac{Z_{\text{cold}}}{Z_\odot} \right) \left( \frac{A_V}{N_H} \right)_\odot. \quad (2)$$

The above extinction is normalised in such a way that gas with solar metallicity,  $Z_\odot = 0.02$ , has the local interstellar medium (ISM) dust-to-gas ratio (e.g. Guiderdoni & Rocca-Volmerange 1987). The neutral hydrogen column density is related to the projected central surface gas mass in the disk,  $M_{\text{cold}}/(2\pi h_R^2)$ , and thus:

$$\tau_{V_0} = 0.043 \left[ \frac{M_{\text{cold}}}{2\pi h_R^2} \frac{pc^2}{M_\odot} \right] \left( \frac{Z_{\text{cold}}}{0.02} \right). \quad (3)$$

The extinction optical depth,  $\tau_{V_0}$ , is obtained in the same way independently of which extinction curve is being used afterwards for the calculation of the attenuation.

Fig. 1 shows the normalised optical depth in the UV to

near IR wavelength range, for the extinction curves from the MW and SMC used by Ferrara et al. (1999) to estimate the attenuation curves of galaxies. For comparison, Fig. 1 also displays the attenuation curve empirically derived from observations of nearby UV-bright, starburst galaxies by Calzetti et al. (2000). For wavelengths  $\lambda \geq 0.35\mu\text{m}$ , the three curves are roughly consistent with each other. However, at smaller wavelengths the SMC extinction curve displays much higher extinction than both the MW and Calzetti curves. The MW extinction curve presents a bump at  $\lambda \sim 2175\text{\AA}$  that is not seen in the other two curves. The presence of this bump is related to the existence of small carbonaceous particles that could be destroyed by the ambient UV radiation field (Fischera & Dopita 2011). Though less pronounced, such a bump has been observed in the Large Magellanic Cloud (Gordon et al. 2003) and in nearby star-forming galaxies (over 23000 galaxies at  $z \sim 0.07$ , Wild et al. 2011). However, the bump at  $\lambda \sim 2175\text{\AA}$  was not detected in the sample of 39 starburst galaxies analysed by Calzetti et al. (1994, 2000). It is worth noting here that Vihj et al. (2003), using a radiative transfer calculation, found the Calzetti attenuation law curve in the particular case of assuming  $\tau_{V_0} = 1.5$  and a clumpy dusty shell with a SMC extinction curve.

### 2.1.2 Molecular clouds

In the model, stars are assumed to form in molecular clouds from which they will eventually leak out. The attenuation of starlight by dust in molecular clouds is calculated analytically, assuming new born stars to be a point source in the centre of a spherical cloud with uniform density.

The attenuation by clouds depends both on the fraction of light produced within the cloud and the extinction optical depth. The light produced within molecular clouds depends on the star formation and chemical enrichment history, the IMF and the wavelength. The attenuation by clouds mostly affects the UV light, which is mainly produced by young stars with a short lifetime. Thus, the fraction of light produced within a cloud is obtained by assuming the recent star formation rate to be either constant in the case of quiescent disks or to decay exponentially for bursts of star formation.

The extinction optical depth is calculated from the column density of gas through a cloud, assuming the same extinction law as for the diffuse component of dust.

As expected, the attenuation calculated in this way depends on wavelength, the metallicity of the gas and the surface density of the clouds, which, in turn, depends on the cloud mass and radius. For further details see Lacey et al. (2012, in prep).

The values of the parameters affecting the dust attenuation calculation in molecular clouds are set to be the same as in the Baugh et al. model. The time for stars to escape from their birth molecular clouds is set to  $t_{\text{esc}} = 1$  Myr and the fraction of dust in molecular clouds to  $f_{\text{cloud}} = 0.25$ . The value of  $f_{\text{cloud}}$  is consistent, within a factor of 2, with estimations based on observations of nearby galaxies (Granato et al. 2000). The value of  $t_{\text{esc}}$  was chosen in order to reproduce the luminosity function of observed LBGs at  $z = 3$ . Moreover, the chosen value for  $t_{\text{esc}}$  is consistent with the escape time inferred from observations of stars in the MW (Leisawitz & Hauser 1988). By default, the mass

of clouds is set to be  $M_{\text{cloud}} = 10^6 M_{\odot}$  and their radius to  $r_{\text{cloud}} = 16$  pc, to match the choices made in GRASIL (Silva et al. 1998), that, in turn, were made to match observations of giant molecular clouds in the MW and to fit the spectral energy distributions (SED) of nearby galaxies. With these parameters the far-UV light of stars within molecular clouds is almost completely extinguished. Thus, the net attenuation by clouds is insensitive to the exact value of the surface density of a single cloud, which is proportional to  $M_{\text{cloud}}/r_{\text{cloud}}^2$ , and it will only depend weakly on the assumed shape of the extinction curve used in the calculation of dust attenuation in molecular clouds.

### 2.1.3 Dust to metals ratios

In GALFORM, a fixed fraction of the total heavy elements in the gas component is assumed to be locked up in dust grains. The dust to metal ratio is thus also fixed in the model. The model uses an instantaneous recycling approximation. This approximation is reasonable as most metals are produced by Type II SNe. Even at high redshifts, an appreciable difference in returned mass fraction only persists for less than  $10^{7.5}$  yr (Nagashima et al. 2005). No attempt is made to model in detail the formation and destruction of dust grains.

In principle, the dust to metal ratio depends on the dust production mechanism, which in turn depends directly on the star formation history of a galaxy. A consensus on the dust production mechanism at different redshifts has not yet been reached and thus, assuming a fixed dust to metal ratio is a reasonable approximation. At low redshift, the bulk of the dust is thought to be generated by stars in the asymptotic giant branch (AGB) phase. Valiante et al. (2009) estimated that even at  $z \sim 6.4$  between 50 and 80 per cent of the total dust mass could be generated by AGB stars. This percentage depends strongly on the assumed star formation history. AGB stars need to reach on average an age of 400 Myr before they produce dust. Thus, at higher redshifts,  $z \geq 6.5$ , there is not enough time for typical AGB stars to generate the dust that has been observed in some systems (Dwek et al. 2007; Michałowski et al. 2010). Although SNe can generate large amounts of dust they also destroy it in shocks (Bianchi & Schneider 2007). The most plausible explanation for the observed dust at  $z \geq 6.5$  appears to be the dust growth in the ISM generated within dense molecular clouds (Michałowski et al. 2010; Dwek & Cherchneff 2011; Valiante et al. 2011).

## 2.2 IGM attenuation

The neutral hydrogen in the IGM absorbs and scatters photons from both the Lyman series (bluewards of  $1216\text{\AA}$ ) and the Lyman continuum<sup>2</sup>. Within GALFORM this effect can be implemented following the attenuation prescriptions of either Madau (1995) or Meiksin (2006). The predicted attenuation at  $1000\text{\AA}$  due to the IGM increases from about 0.5

<sup>2</sup> The absorption due to the Helium present in the IGM is, in general, negligible compared with that by neutral hydrogen at the wavelengths of interest here.

magnitudes at  $z \sim 4$  to 2 magnitudes at  $z \sim 6$ , with either prescription.

Madau (1995) used an empirical approach to model the IGM attenuation, while Meiksin based part of the prescription on the results of a  $\Lambda$ CDM simulation with similar cosmological parameters to those used in the B05 model. Numerical simulations have proved to be successful at reproducing different observational properties of absorbing systems.

The effective optical depth through the IGM depends on the number of absorbers, basically neutral hydrogen clouds, along the line of sight. Each absorber is characterised by its redshift, its neutral hydrogen column density,  $N_{\text{HI}}$ , and its Doppler parameter, which is related to the temperature and kinematics of the cloud. The absorption of the Lyman continuum is mainly caused by Lyman limit systems (LLSs), with  $N_{\text{HI}} \sim 10^{17}\text{cm}^{-2}$  and scattering by the Lyman  $\alpha$  forest (LAF), optically thin systems at the Lyman edge, with  $N_{\text{HI}} \sim 10^{13}\text{cm}^{-2}$ .

Madau and Meiksin assumed different evolution with redshift for the number of LAF and LLSs. While Madau considered that the LAF followed a Poisson distribution, Meiksin obtained the LAF distribution from a N-body cosmological simulation.

An empirical evolution of LLSs with redshift is assumed by both Madau and Meiksin. However, only the latter is consistent with current observations in the redshift range  $0.3 \lesssim z \lesssim 4$  (see Fig. 3 in Inoue & Iwata 2008).

Another important difference between the Madau and Meiksin modelling of the intergalactic attenuation is that in the former a fixed Doppler parameter is assumed, while Meiksin varies this value based on simulations, a change supported by several observational studies (e.g. Kim et al. 1997). Moreover, the Madau model almost always predicts a smaller transmission than empirical models based on the most recent observations (see Fig. 6 in Inoue & Iwata 2008).

In light of the above discussion, the results presented in this paper are calculated by default using the Meiksin (2006) equations.

## 3 LYMAN-BREAK SELECTION FOR GALAXIES AT HIGH REDSHIFTS

Observationally, the most extensively used method for selecting star-forming galaxies at high redshifts is the Lyman drop-out technique (for details on other methods see the review by Dunlop 2012). This technique uses near-UV, optical and near-IR filters (depending on the target redshift) to sample the redshifted Lyman-break, thereby selecting star-forming galaxies, the so called Lyman Break Galaxies (LBGs). This method has been commonly applied to select galaxies with  $z > 2.5$ , since their Lyman-break is shifted beyond the observed frame UV range that is difficult to observe with ground-based telescopes.

The drop-out technique typically uses 2 colours, one from filters bracketing the Lyman-break and the second quantifying the UV continuum slope. The rest-frame UV emission,  $300 \leq \lambda(\text{\AA}) \leq 3000$ , is largely due to the presence of young and massive OB stars in galaxies. Thus, the rest-frame UV emission of galaxies that are not actively forming stars is, in general, negligible in comparison with that in

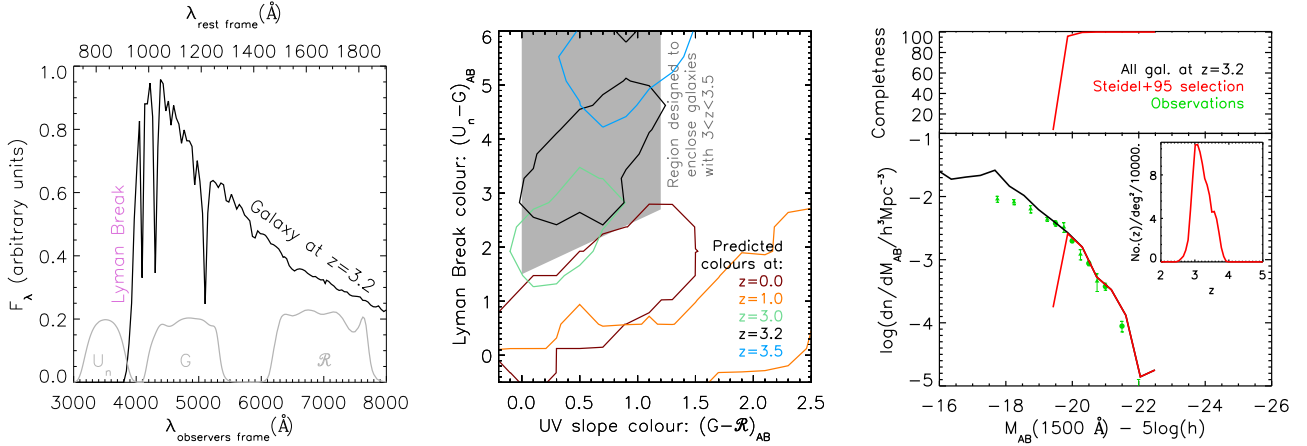


**Figure 2.** An illustration of the drop-out technique used to select galaxies at  $3 < z < 3.5$ . *Left panel:* The intrinsic spectrum of a star-forming galaxy at  $z = 3.2$ , computed with the PEGASE.2 population synthesis model (Fioc & Rocca-Volmerange 1997) (black line, no attenuation is included) plotted together with the response functions of the  $U_n$ ,  $G$  and  $\mathcal{R}$  filters (grey lines). *Central panel:* The  $(U_n-G)$  versus  $(G-\mathcal{R})$  colour-colour plot proposed by Steidel et al. (1995) for selecting galaxies at  $3 < z < 3.5$  (grey region) with the predicted density contours for galaxies at different redshifts, as indicated in the legend. The density contours enclose 80 per cent of the galaxies brighter than  $\mathcal{R} < 25.5$  and  $G < 27.29$  at each redshift. *Right panel:* The predicted completeness (top panel) and luminosity function (main panel) at  $z = 3.2$  of all galaxies (black line) and galaxies with  $\mathcal{R} < 25.5$  and  $G < 27.29$  and the colour cuts shown in the central panel as a grey region (red lines). The redshift distribution of this last subsample is shown in the inset. For comparison, we show as green symbols the observed luminosity function from Sawicki & Thompson (2006) (triangles,  $1700\text{\AA}$ ), and Reddy & Steidel (2009) (circles,  $1700\text{\AA}$ ).

star-forming galaxies. The Lyman-break is the result of both the Lyman-limit break (at  $912\text{\AA}$ ) due to neutral hydrogen in the atmospheres of massive stars and the Lyman- $\alpha$ -break (at  $1216\text{\AA}$ ) due to absorption by intervening neutral gas clouds (e.g. the Lyman- $\alpha$  forest).

The drop-out technique was first proposed by Steidel & Hamilton (1992), using the  $U_n$ ,  $G$  and  $\mathcal{R}$  filters shown in Fig. 2. The grey area in the central panel of Fig. 2 shows the selection criteria used by Steidel et al. (1995) to select galaxies at  $3 < z < 3.5$ . The left panel in Fig. 2 shows the synthetic spectrum of a star-forming galaxy at  $z = 3.2$ , computed with the PEGASE.2 stellar population synthesis model (Fioc & Rocca-Volmerange 1997) without including the attenuation by either dust or the IGM. This spectrum shows a very pronounced break at  $912\text{\AA}$  in the rest frame, the Lyman-limit break. Bluewards of this rest-frame wavelength, the galaxy is practically not emitting any light. Thus, by measuring the  $(U_n-G)$  colour of a galaxy it is possible to select candidates at  $3 < z < 3.5$ , since in this redshift range the  $U_n$  band is bluewards of the Lyman-break and the  $G$  band redwards. The  $(G-\mathcal{R})$  colour samples the rest-frame UV continuum slope and is used in order to minimise the number of lower redshift interlopers.

The central panel of Fig. 2 shows, using density contours, the location in the colour-colour plane of the model galaxies at different redshifts. It is clear from this plot that a selection based only on the colour sampling the Lyman-break (i.e.  $(U_n-G)$  in this example) will contain a substantial fraction of galaxies at  $z \sim 0$ . Old and passively evolving galaxies at  $z \sim 0$  present a deep enough break at  $4000\text{\AA}$  to be mistaken for the Lyman-break of star-forming galaxies at higher redshifts. However, the slopes of the spectral continuum redwards of these breaks are very different. The rest-frame optical continuum of old galaxies at  $z \sim 0$  is quite red,

while the rest-frame intrinsic UV continuum of star-forming galaxies is bluer, as shown in the left panel of Fig. 2. Thus, a cut on  $(U_n-G)$  varying with  $(G-\mathcal{R})$  can remove most of the low redshift interlopers. However, the presence of dust in star-forming galaxies at high redshift can redden the  $(G-\mathcal{R})$  colour, resulting in an overlap with the colours of lower redshift galaxies. Thus, these high redshift dusty galaxies would not be classified as LBGs.

The right panel of Fig. 2 shows the luminosity function of model galaxies selected using Steidel et al. magnitude and colour cut criteria, compared with that for all model galaxies at  $z = 3.2$ . This figure shows that the luminosity function of galaxies selected following Steidel et al. criterion is complete above the rest-frame UV absolute magnitude that corresponds to the R-band magnitude limit of the observations. Note that the observational data in the right panel of Fig. 2 goes deeper than the original work from Steidel et al.

The inset in the right panel in Fig. 2 shows the predicted redshift distribution of galaxies with  $\mathcal{R} < 25.5$  and  $G < 27.29$  and colours within the region proposed by Steidel et al. to select galaxies at  $3 \leq z \leq 3.5$ . The model galaxies selected in this way have redshifts in the range  $3 < z < 4$ , in agreement with the selection proposed by Steidel et al.

#### 4 THE PREDICTED DUST ATTENUATION

The presence of even small amounts of dust in high redshift galaxies can have a strong effect on the observed UV light. With the same model as the one used here, Lacey et al. (2011) predicted that dust attenuation in the far-UV ( $\sim 1500\text{\AA}$ ) is typically 2 magnitudes for galaxies dominating the UV luminosity density, even out to redshift 10.

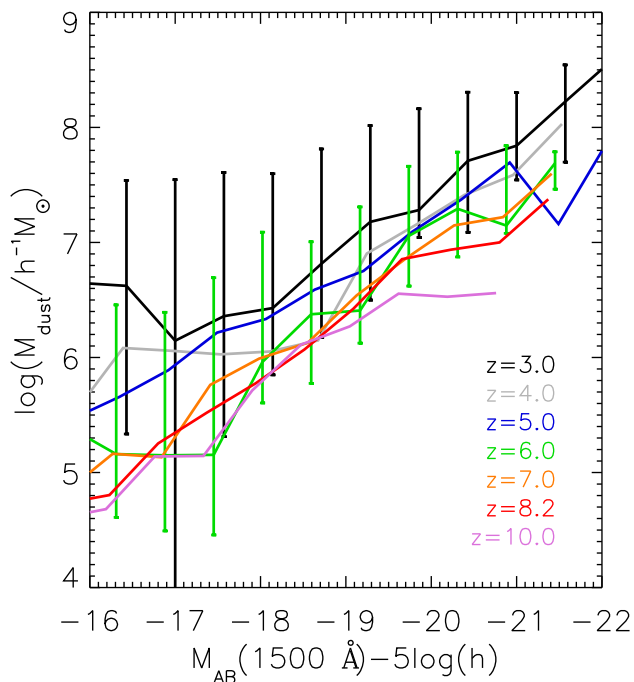


**Figure 3.** Predicted median dust mass as a function of the attenuated absolute rest-frame UV magnitude ( $\sim 1500\text{\AA}$ ) for galaxies at different redshifts, as indicated in the legend. For clarity, the error bars representing the 10 and 90 percentiles are only shown for two redshifts.

Below we present the predicted median dust masses, optical depths and attenuations for galaxies at  $3 \leq z \leq 10$ .

#### 4.1 The predicted dust masses

Following Granato et al. (2000), who used a physical dust grain model, we assume that the dust to gas ratio in clouds and the diffuse ISM is proportional to the gas metallicity,  $Z_{\text{cold}}$ , with a value of  $1/110$  for  $Z = Z_{\odot} = 0.02$ . Thus, the total dust mass in a galaxy,  $M_{\text{dust}}$ , can be calculated as follows:

$$M_{\text{dust}} = \frac{1}{110} X_{\text{H}} M_{\text{cold}} \left( \frac{Z_{\text{cold}}}{0.02} \right), \quad (4)$$

where  $M_{\text{cold}}$  is the total cold gas mass in the galaxy and  $X_{\text{H}} = 0.74$  is the mean hydrogen mass fraction in the Universe.

Fig. 3 shows the predicted median dust mass (Eq.4) as a function of absolute rest-frame UV magnitude for galaxies at redshifts from 3 to 10. There is a clear trend for brighter galaxies to have higher dust masses. This trend is a direct consequence of the predicted relation between the far UV magnitude and gas mass, combined with the fact that the predicted metallicity of cold gas appears to be weakly dependant on luminosity (see Lacey et al. 2011). It is also clear from Fig. 3 that the model predicts a decrease in dust content with increasing redshift. At a given luminosity, we find a decrease in dust mass of a factor of  $\sim 5$  from  $z = 3$  to  $z = 10$  for galaxies with  $-20 \leq M_{\text{AB}}(1500\text{\AA}) - 5\log h \leq -18$ .

Observations of galaxies in the wavelength range from the far IR to the sub-mm have allowed direct estimates of the

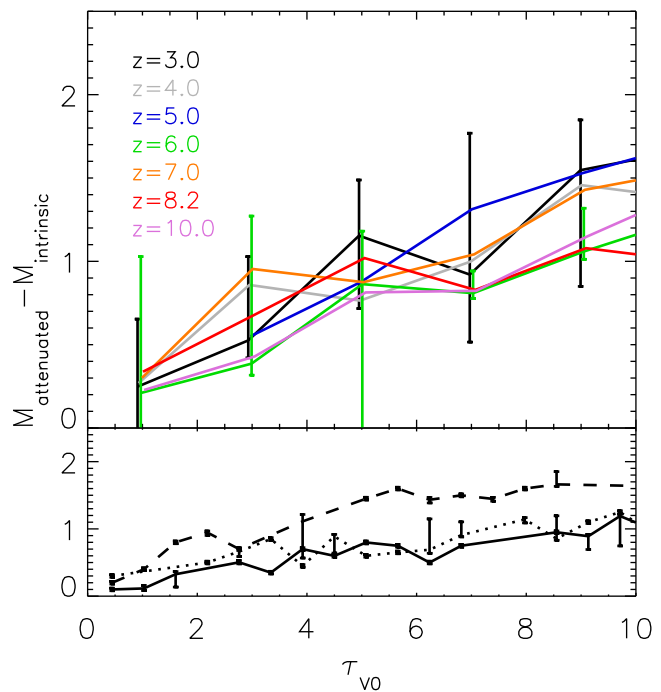


**Figure 4.** The predicted median difference between the attenuated and the intrinsic rest-frame UV magnitude as a function of the central extinction optical depth in the V-band,  $\tau_{V_0}$ , for galaxies with  $M_{\text{AB}}(1500\text{\AA}) - 5\log h < -17.8$ , plotted at the redshifts indicated in the legend. For clarity, the error bars representing the 10 and 90 percentiles are only shown for two redshifts. The *bottom panel* shows the attenuation at  $z = 3$  for galaxies binned in three inclination ranges:  $15^{\circ} \leq i < 20^{\circ}$  (solid line),  $45^{\circ} \leq i < 50^{\circ}$  (dotted line, range bracketing the median value of the sample),  $70^{\circ} \leq i < 75^{\circ}$  (dashed line).

dust mass in some galaxies above  $z \sim 4$ . Dust masses in excess of  $\sim 10^8 h^{-1} M_{\odot}$  have been found in galaxies with stellar masses estimated to be between  $10^{10}$  to  $10^{11} h^{-1} M_{\odot}$  at redshifts  $4 \leq z \leq 5$  and in QSOs up to  $z \sim 6.5$  (McMahon et al. 1994; Dunlop et al. 1994; Robson et al. 2004; Dwek et al. 2007; Michałowski et al. 2010). However, other galaxies at similar redshifts do not present any evidence of containing dust (Zafar et al. 2010). For galaxies within the range of stellar masses  $10^{10}$  to  $10^{11} h^{-1} M_{\odot}$ , we find median dust masses around  $\sim 10^8 h^{-1} M_{\odot}$ , in agreement with those observations which detect dust in high redshift galaxies.

#### 4.2 The predicted optical depth

As described in §2.1, the dust attenuation of starlight is directly related to the extinction central optical depth in the V-band of a galaxy,  $\tau_{V_0}$ . Fig. 4 presents the median predicted attenuation in the UV as a function of  $\tau_{V_0}$  for galaxies with  $M_{\text{AB}}(1500\text{\AA}) - 5\log h < -17.8$  (corresponding to a tenth of the characteristic luminosity at  $z = 3$  as reported by Steidel et al. 1999). Despite the scatter, there is a clear trend for galaxies with higher extinction optical depths to present higher UV attenuations. This trend is found to be independent of redshift, in the studied range  $3 \leq z \leq 10$ . We find the median optical depth of galaxies brighter than  $M_{\text{AB}}(1500\text{\AA}) - 5\log h < -17.8$  to be between 2 and 6. These

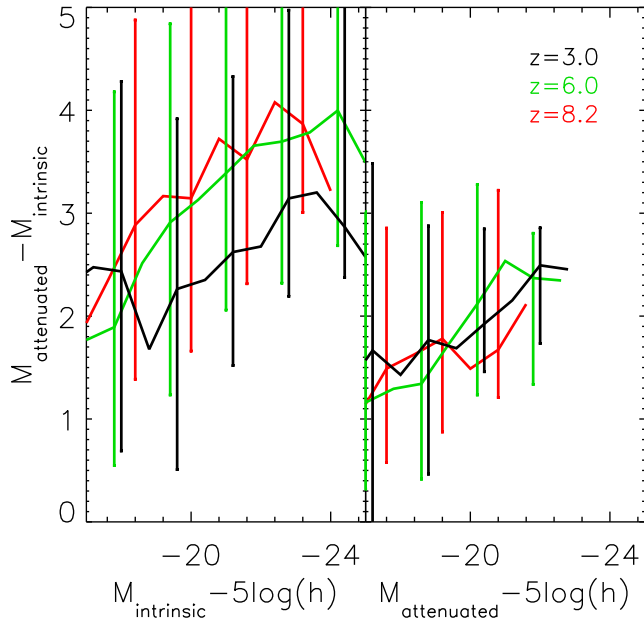


**Figure 5.** The median attenuation in magnitudes at  $1500\text{\AA}$  as a function of intrinsic (left panel) and attenuated (right panel) absolute UV ( $1500\text{\AA}$ ) magnitude for model galaxies at  $z \sim 3$  (black), 6 (green) and 8.2 (red). The error bars show the 10 and 90 percentiles for the distribution.

median values depend strongly on the magnitude cut applied to select the galaxies. We also find that brighter galaxies present higher extinction optical depths, though this trend has a large scatter.

### 4.3 The predicted median UV attenuation

The attenuation of starlight depends not only on the extinction central optical depth but also on the inclination of the galaxy, the distribution of the dust and the fraction of dust in molecular clouds. The lower panel in Fig. 4 shows that when galaxies are selected within small ranges of inclination, the attenuation-optical depth relation shows little scatter, with the attenuation increasing as the inclination increases towards the edge-on case.

Fig. 5 shows the median attenuation of model galaxies at  $z = 3, 6$  and  $8.2$ , as a function of both the intrinsic and attenuated UV absolute magnitude. In both cases a trend can be seen for brighter galaxies to be more attenuated, though this is dominated by scatter, especially for attenuated UV magnitudes. The large scatter found suggests that, in general, the attenuation is not related in a simple way with the UV magnitude.

Fig. 6 is similar to Fig. 5 but for the subsample of LBGs at  $z = 3, 6$  and  $8.2$ , selected by applying (to the attenuated colours) the magnitude and colour selection of Steidel et al. (1995), Bouwens et al. (2012) and Lorenzoni et al. (2011), respectively. Fig. 6 shows that the range of absolute magnitude covered by these galaxy selections is different. As was shown in Fig. 2, the LBGs selected by Steidel et al. criteria are bright galaxies, with  $M_{\text{AB}}(1500\text{\AA}) - 5\log h \leq -20$ . The selections from both Bouwens et al. and Lorenzoni et al. make use of the deep HST photometry, sampling fainter

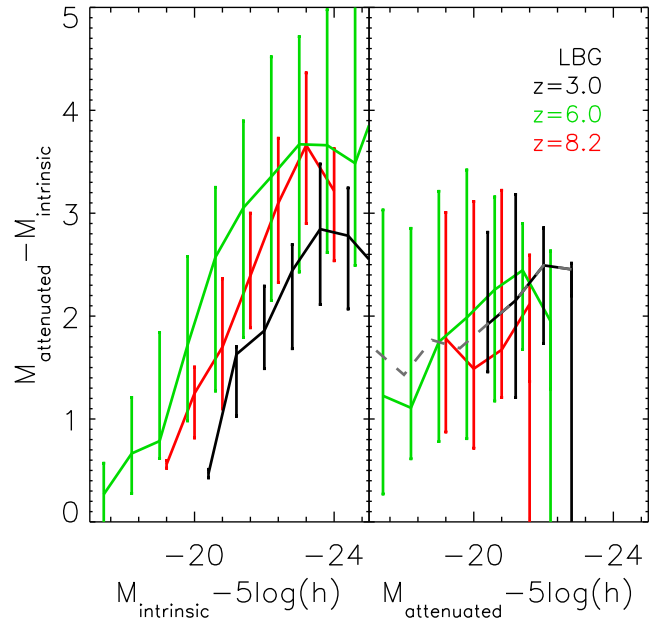


**Figure 6.** Figure similar to Fig. 5 but for the subsample of model galaxies which pass various LBG colour and magnitude selections at  $z \sim 3$  (selection from Steidel et al. 1995, black), 6 (selection from Bouwens et al. 2012, green) and 8.2 (selection from Lorenzoni et al. 2011, red). For comparison, the median attenuation for all galaxies at  $z = 3$ , shown in Fig. 5, is included here as a grey dashed line. The error bars show the 10 and 90 percentiles of the distribution.

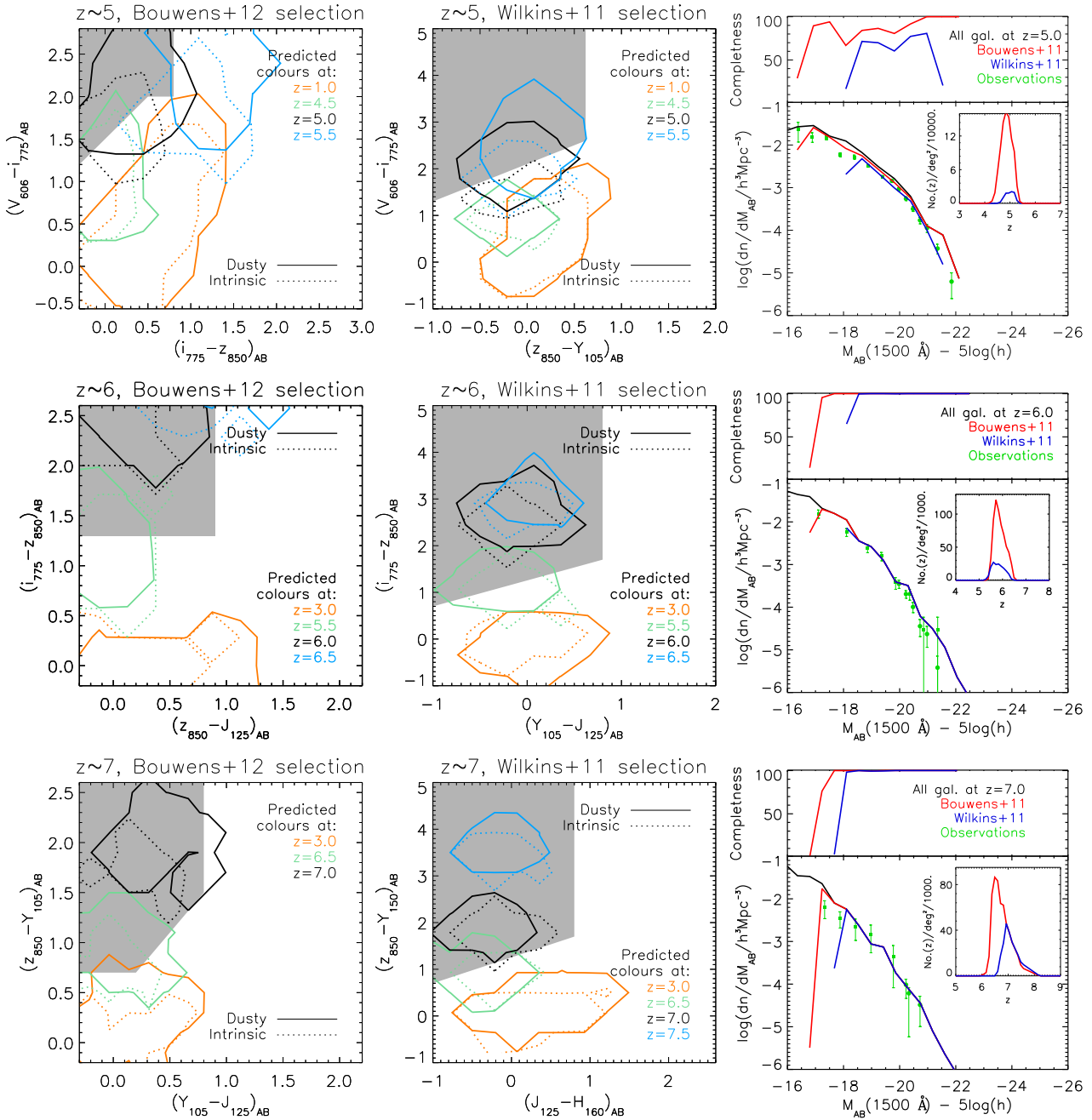
galaxies. In the next section we will explore these selections further, comparing them with the model predictions.

Fig. 6 shows clearly that intrinsically brighter LBGs tend to be more attenuated at all redshifts. However, when plotting against the attenuated UV luminosity, the trend is weakened, being dominated by the scatter. A direct estimation of the attenuation in high redshift galaxies spanning the range from 0 to 5, similar to that predicted, has recently been made using results from *Herschel* (Burgarella et al. 2011; Buat et al. 2012; Lee et al. 2012; Reddy et al. 2012).

The right panel in Fig. 6 remains virtually unchanged if we only apply the cuts in apparent magnitude from the observational surveys (see the Appendix for the specific values). This suggests that the LBG colour selection does not lead to an appreciable bias in average UV attenuation of the sample. In fact, the right panel in Fig. 6 shows the complete overlap at  $z = 3$  between the median attenuation of all galaxies and that for LBGs, at least within the magnitude range where the latter are selected.

## 5 THE PREDICTED UV COLOURS OF LBGs

We start our study of the predicted rest-frame UV colours of LBGs by comparing the locus occupied by model galaxies with the colour region designed by observers to implement the Lyman drop-out technique. Usually, these colour-colour regions are constructed by following the colour evolution of model starburst galaxies with a range of negative UV continuum slopes, predicted using a stellar population synthesis (SPS) model. Figs. 2, 7 and 8 show as grey areas some exam-



**Figure 7.** The *left* and *central* columns show the predicted density contours for model galaxies at the redshifts indicated in the legend, in the colour-colour space defined by Bouwens et al. (2012) (left) and Wilkins et al. (2011b) (centre) to select LBGs at  $z = 5$  (top row),  $z = 6$  (middle row) and  $z = 7$  (bottom row) [grey areas in each plot]. The density contours enclose 80 per cent of galaxies brighter than the limits set by the different observational studies (see the Appendix). The solid/dotted contours correspond to colours with/without considering the dust attenuation. The *right* column shows as black lines the predicted completeness and luminosity function of all galaxies at these redshifts. The blue/red lines correspond to the predicted completeness and luminosity function for the subsample obtained using the selection criteria from Wilkins et al. (2011b)/Bouwens et al. (2012), the predicted redshift distributions of these subsamples are shown in the insets of the right column. For comparison, in the right column we also show in green the observed luminosity function from: Bouwens et al. (2007) (squares,  $1600 \text{ \AA}$ ) and McLure et al. (2009) (circles,  $1500 \text{ \AA}$ ) at  $z = 5$  (top); Bouwens et al. (2007) (squares,  $1350 \text{ \AA}$ ) and McLure et al. (2009) (circles,  $1500 \text{ \AA}$ ) at  $z = 6$  (middle); McLure et al. (2010) (squares,  $1500 \text{ \AA}$ ) and Ouchi et al. (2009) (circles,  $1500 \text{ \AA}$ ) at  $z = 7$  (bottom).

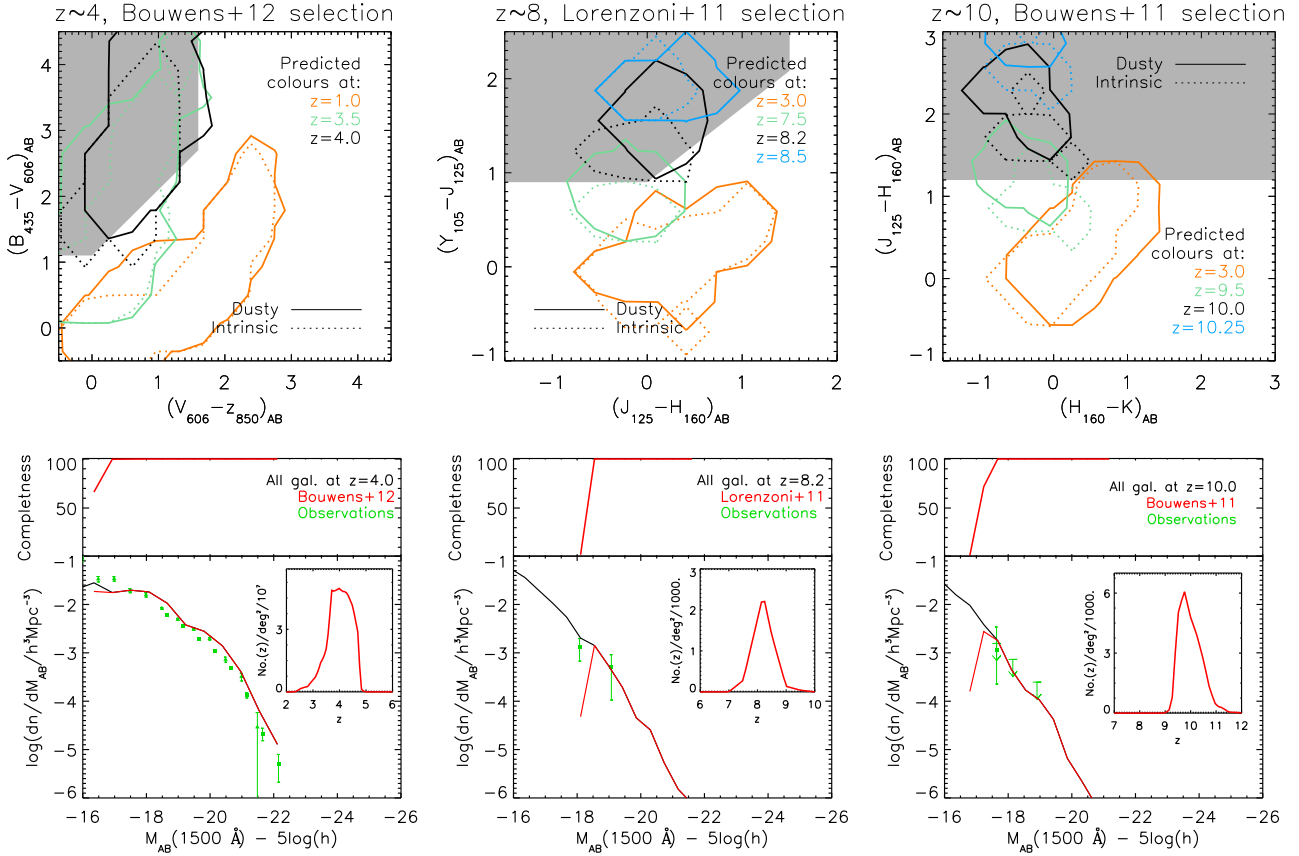


**Figure 8.** *Top row:* The predicted density contours for model galaxies at the redshifts indicated in the legend, in the colour-colour space defined by the Bouwens et al. (2012) (left) Lorenzoni et al. (2011) (centre) and Bouwens et al. (2011) (right) to select LBGs at  $z = 4$ ,  $z = 8.2$  and  $z = 10$ , respectively (grey areas in each plot). The density contours enclose 80 per cent of galaxies brighter than the limits set by the different observational studies (see the Appendix). *Bottom row:* The black lines show the predicted completeness and luminosity function of all galaxies at  $z = 4$  (left),  $z = 8.2$  (centre) and  $z = 10$  (right). The red lines correspond to the predicted completeness and luminosity function at the same redshifts for the subsample obtained using the selection criteria from Bouwens et al. (2012) (left), Lorenzoni et al. (2011) (centre) and Bouwens et al. (2011) (right). The predicted redshift distributions of these subsamples are shown in the insets (note that the y-axis units in the left panel are  $\text{No.}(z)/\text{deg}^2/10^7$ ). For comparison, we also show in green the observed luminosity function from: Yoshida et al. (2006) ( $z \sim 4$ , squares,  $1500 \text{ \AA}$ , left), Bouwens et al. (2007) ( $z \sim 4$ , triangles,  $1600 \text{ \AA}$ , left), McLure et al. (2010) ( $z \sim 8.2$ ,  $1500 \text{ \AA}$ , centre) and Bouwens et al. (2011) ( $z \sim 10$ ,  $1600 \text{ \AA}$ , right).

ples of such colour selection regions<sup>3</sup>. In most cases, the observational data points are distributed covering most of the drop-out region. In these figures, we compare the observationally designed drop-out regions with the density contours for model galaxies brighter than the limiting magnitudes in the corresponding observational studies (see the Appendix for a list of the selection criteria used in different studies). As we can see in Figs. 2, 7 and 8, the predicted UV colours of bright galaxies at  $2.5 \leq z \leq 10$  are consistent with the colour selection regions designed observationally.

In each of the colour-colour panels in Figs. 2, 7 and 8, the location of model galaxies at a range of redshifts, beyond the target one, are shown to assess whether or not there are interlopers. In these figures we also present the predicted redshift distribution of the galaxies selected following the

magnitude and colour cuts from the observational studies (see the Appendix). These predicted redshift distributions agree with the target redshifts of each selection.

As can be seen in Figs. 2, 7 and 8, the predicted luminosity functions of those galaxies selected following the application of the magnitude and colour cuts described in the different observational studies are in very good agreement with observations up to  $z \sim 10$ . This is remarkable, since the Baugh et al. (2005) model was designed considering only LBGs at  $z = 3$ . Lacey et al. (2011) presented a detailed study of the physical processes affecting the predicted evolution of the UV luminosity function and a comparison with observational results.

Fig. 7 shows that, with the HST filter set, it is particularly difficult to select a complete sample of galaxies at  $z = 5$  whilst at the same time attaining a minimum fraction of low redshift interlopers. As previously reported by Bouwens et al. (2012), the expected locus of galaxies at  $z = 5$  in the colour-colour plot designed for the drop-out technique partially overlaps that for galaxies at lower redshifts. Thus, in order to minimise the fraction of low red-

<sup>3</sup> HST bands used here are F435W, F606W, F775W, F850LP, F105W, F125W, F160W (hereafter  $B_{435}$ ,  $V_{606}$ ,  $i_{775}$ ,  $z_{850}$ ,  $Y_{105}$ ,  $J_{125}$ ,  $H_{160}$ , respectively). The transmission curves of these filters can be seen in Fig. 10.

shift interlopers, the completeness of the high- $z$  selection is reduced. At  $z = 5$  we predict that the drop-out selection proposed by Wilkins et al. (2011b) recovers  $\sim 70$  per cent of all galaxies with  $-21.5 \leq M_{AB}(1500\text{\AA}) \leq -18.5$ , and that from Bouwens et al. (2012)  $\sim 85$  per cent. Figs. 2, 7 and 8 show that the predicted completeness of the drop-out selection recovers more than 90 per cent of the galaxies brighter than the absolute magnitude implied by the apparent magnitude observational limits at  $z = 3, 4, 6, 7, 8$  and 10. Similar completeness are also found for the predicted galaxies at  $z = 2.5$ .

Next we explore how the predicted UV colours change when different model parameters are varied. In particular, we explore the effect of changing the stellar population synthesis (SPS) model and the attenuation by both the IGM and dust.

### 5.1 The effect of changing the SPS model

The Baugh et al. (2005) model uses by default the simple stellar populations generated by Bressan et al. (1998), using the Padova 1994 stellar evolutionary tracks<sup>4</sup> and the model stellar atmospheres from Kurucz (1993)<sup>5</sup>. We have compared the UV colours predicted using the default SPS model with those from PEGASE.2 (Fioc & Rocca-Volmerange 1997), Maraston (2005) and Conroy et al. (2009). The SPSs models from both Maraston and Conroy et al. use stellar evolutionary tracks including a model for the Thermally-Pulsating Asymptotic Giant Branch phase of stellar evolution that can reproduce observations better than previous attempts to model this stellar phase. Conroy et al. also included a post-AGB phase and an extended blue horizontal branch for stellar evolution, matching UV observations of old star clusters.

The effect that stars in the Thermally-Pulsating Asymptotic Giant Branch phase have on the UV colours of a galaxy is negligible, since these stars are mainly bright in the near IR. Though bright in the UV, stars only reach a post-AGB phase at ages much older than those of the LBGs. Thus, little variation is expected in the UV colours predicted on using different SPS models. Indeed, we find that the UV colours of LBGs predicted using the different SPS models are consistent with each other.

### 5.2 The effect of the IGM on the UV colours

As described in §2.2, the IGM attenuates the UV light, mainly at wavelengths  $\lambda < 1216\text{\AA}$ , and has a larger effect at higher redshifts. Fig. 9 shows as density contours the predicted rest-frame UV colours for galaxies at  $z = 4$  with and without taking into account the effect of the IGM attenuation. At  $z \geq 3$ , the colours sampling the Lyman-break change by more than 0.5 magnitudes when the IGM attenuation is included. In Fig. 9 we can see such change at  $z = 4$ . It is clear the need to take into account the effect of the

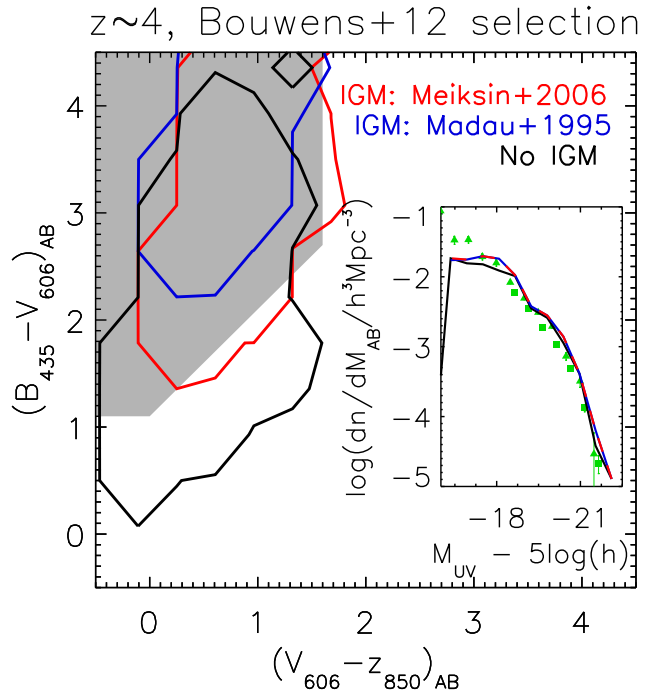


**Figure 9.** The  $(B_{435}-V_{606})_{AB}$  versus  $(V_{606}-z_{850})_{AB}$  colour-colour plot proposed by Bouwens et al. (2012) for selecting galaxies at  $z \sim 4$  (grey region) together with the predicted density contours for galaxies at  $z = 4$ . The density contours enclose 80 per cent of galaxies with  $V_{606} < 30.1$  and  $z_{850} < 29.4$ . The inset shows the predicted luminosity function for galaxies selected at  $z = 4$  with  $V_{606} < 30.1$ ,  $z_{850} < 29.4$  and the colour cuts shown by the grey region in the colour-colour plot. In both cases, the black lines correspond to the predictions without considering the IGM attenuation and the blue/red lines to those predictions made using the Madau (1995)/Meiksin (2006) prescriptions for the IGM attenuation. Note that the predicted luminosity functions using either IGM prescription are the same at this redshift. For comparison, we show in green the observed luminosity function from Yoshida et al. (2006) (squares,  $1500\text{\AA}$ ) and Bouwens et al. (2007) (triangles,  $1600\text{\AA}$ ).

IGM attenuation when studying the rest frame UV colours of high redshift galaxies.

Fig. 9 also shows the distribution of model galaxies when either the Madau (1995) or the Meiksin (2006) prescription is used to model the IGM attenuation. In §2.2 we pointed out that the prescription of Madau shows a smaller transmission than that of Meiksin. This implies that the predicted colours sampling the Lyman-break are expected to be slightly redder for the model using the Madau prescription. Fig. 9 illustrates this difference for galaxies at  $z = 4$ . Nevertheless, the difference in the predicted rest-frame UV colours is found to be small. In fact, we do not find a significant difference in the luminosity function of LBGs modelled using either IGM attenuation prescription for galaxies at  $2.5 \leq z \leq 10$  (see the inset in Fig. 9 for the case of  $z = 4$  and LBGs selected following Bouwens et al. 2012).

In our model, reionisation is assumed to be instantaneous. Indeed, analyses of the line of sight to quasars at  $z > 6$  are consistent with a uniformly ionised IGM at  $z \sim 6$

<sup>4</sup> <http://stev.oapd.inaf.it/cgi-bin/cmd>,  
<http://pleiadi.pd.astro.it/>.

<sup>5</sup> These are close to the isochrones and stellar atmospheres used by Bruzual & Charlot (2003).

(e.g. Schroeder et al. 2012). At higher redshifts, numerical simulations of reionisation suggest a gradual process, implying the existence of ionised bubbles in a mainly neutral medium (Benson et al. 2001; Iliev et al. 2006). The fact that the predicted luminosity function including the effect of the IGM matches the observations suggests that a minimal fraction of galaxies would not be detected due to the possible patchiness of the IGM at very high redshifts.

### 5.3 Dust treatment and the UV colours

In Figs. 7 and 8 we compare the predicted distributions of UV colours with and without considering the effect of dust. As can be seen there, in general, the presence of dust increases the spread of UV colours. At  $z = 5$ , the inclusion of dust clearly makes galaxies redder in the colour sampling the Lyman-break for both the Bouwens et al. (2012) and Wilkins et al. (2011b) colour selections. At this redshift most galaxies would be missed by these two drop-out techniques if intrinsic colours were going to be used. As mentioned before, using the HST bands, the selection of LBGs at  $z = 5$  needs to be done using stringent colour cuts, in order to minimise low redshift interlopers. The effect of dust on the UV colours at other redshifts,  $z \neq 5$ , is not so strong and approximately the same completeness is recovered using the predicted galaxy colours with and without considering the effect of dust.

Next we explore the effects that changing some of the model parameters controlling the dust treatment have over the predicted rest-frame UV colours.

#### 5.3.1 Changing the extinction law

The extinction curve of a galaxy is determined by the composition and size distribution of the galactic dust, which in turn depends directly on the star formation history of a galaxy. At high redshift it is particularly unclear which mechanism produced the bulk of the observed dust (Bianchi & Schneider 2007; Valiante et al. 2009; Michałowski et al. 2010; Dwek & Cherchneff 2011; Valiante et al. 2011) and thus which extinction curve best describes high redshift galaxies. Here, the dust attenuation calculation is based on the results of the radiative transfer model of Ferrara et al. (1999), which assumes a particular extinction curve as an input.

Fig. 10 shows for 8 galaxies, the effective optical depth as a function of wavelength, obtained using 42 narrow, 50Å, top-hat filters starting with either the MW extinction curve (the default one in the model) or the SMC extinction curve. These 8 galaxies are at  $z = 4$ , they are bright,  $z_{850} > 29.4$ , they have inclinations between 55 and 65 degrees and they have been selected as they exhibit different attenuations in the  $z_{850}$  band. We can see from this figure that the main features of both the MW and SMC extinction curves, namely the bump at 2175Å for the MW curve and the stronger UV extinction at smaller wavelengths in the SMC curve, are still visible after the radiative transfer calculation, which takes into account the distribution of dust in the galaxies and the viewing angle. As we can see in Fig. 10, the characteristics of the assumed extinction curve affect the inferred dust attenuation. This result stresses the relevance of understanding

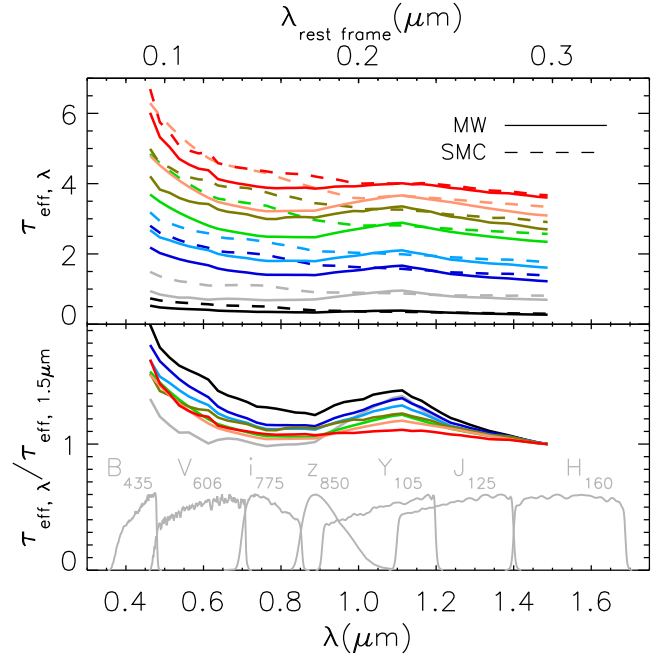


**Figure 10.** *Top panel:* The optical depth as a function of wavelength for 8 galaxies at  $z = 4$  with different UV attenuations, obtained using 42 narrow top-hat filters starting with either the MW extinction curve (solid lines) or the SMC curve (dashed lines). *Bottom panel:* The optical depth normalised at  $1.5\mu\text{m}$  for those galaxies in the top panel (each galaxy is presented as a line of the same colour in both panels). For reference, also shown are the response functions of the HST filters used to select LBGs at different redshifts (lower set of grey curves).

better the characteristics of dust distribution when interpreting observational results.

The lower panel in Fig. 10 shows the effective optical depth normalised to that at  $1.5\mu\text{m}$ , when starting with a MW extinction curve. This panel shows clearly how the features in the attenuation curves get smoother for higher attenuations. The same is seen if we start with a SMC extinction curve for dust in both the diffuse phase and in molecular clouds.

Fig. 11 shows the distribution of model galaxies in the colour-colour plot proposed by Bouwens et al. (2012) to select galaxies at  $z \sim 6$  (grey area) when different input extinction curves are used. The model galaxies populate the region designed to select galaxies at  $z \sim 6$ , independently of the input extinction curve. However, the median UV continuum slope is redder if we start with a SMC extinction law. We will return to this point in section §6.

The inset in Fig. 11 shows that the luminosity function of LBGs at  $z=6$  (selected following Bouwens et al. 2012) predicted from the model using the SMC extinction law is about half a magnitude fainter than that using the MW extinction law. The luminosity function of all galaxies at  $z = 6$  starting the calculations with either the SMC or the MW extinction curves still show this difference and, thus, it cannot be due to the colour cuts applied in the LBG selection. This difference is due to the fact that the SMC curve, as shown in Fig. 1, produces a larger attenuation in the rest-frame UV range than is obtained from the MW curve.

As discussed in Lacey et al. (2011), the UV luminosity

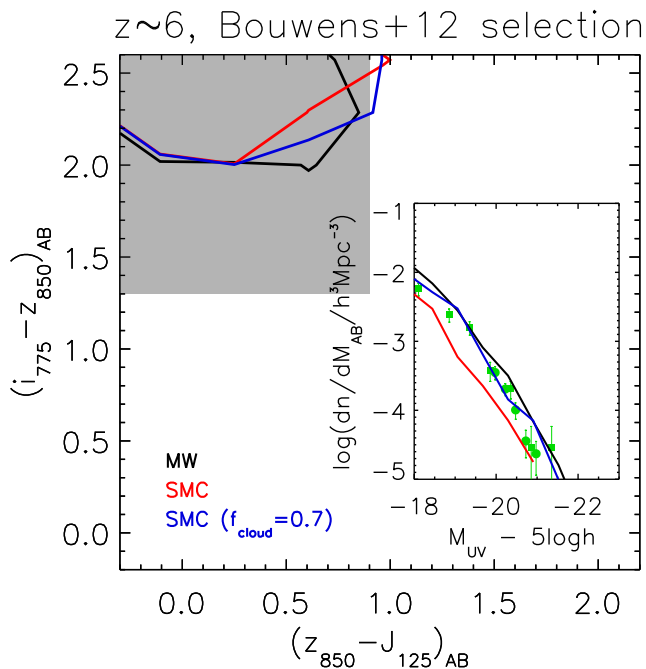


**Figure 11.** The  $(i_{775}-z_{850})_{AB}$  versus  $(z_{850}-J_{125})_{AB}$  colour-colour plot proposed by Bouwens et al. (2012) to select galaxies at  $z \sim 6$  (grey region) with the density contours for model galaxies at  $z = 6$ . The density contours enclose 80 per cent of galaxies with  $z_{850} < 29.4$  and  $J_{125} < 29.9$ . The inset shows the predicted luminosity function for galaxies selected at  $z = 6$  with  $z_{850} < 29.4$  and  $J_{125} < 29.9$  and the colour cuts shown as a grey region in the colour-colour plot. In both cases, the black lines corresponds to the default case of using the MW extinction law, the red to using the SMC extinction law and the blue lines corresponds to predictions made using the SMC extinction law and adopting  $f_{\text{cloud}} = 0.7$  (where the default value is  $f_{\text{cloud}} = 0.25$ ). For comparison, we show in green the observational data from Bouwens et al. (2007) (squares, 1350Å) and McLure et al. (2009) (circles, 1500Å).

function is very sensitive to the fraction of dust in molecular clouds,  $f_{\text{cloud}}$ , and the time that is assumed for stars to migrate out of clouds,  $t_{\text{esc}}$ . Increasing  $f_{\text{cloud}}$  or decreasing  $t_{\text{esc}}$  has the effect of reducing the dust attenuation. By default, it is assumed that 25 per cent of the dust is locked up in molecular clouds and that new stars will migrate out of these after 1Myr. From MW observations, this escape time is found to be between 1 and 3 Myr (Leisawitz & Hauser 1988). Thus, further reducing  $t_{\text{esc}}$  might be unrealistic. However, increasing the amount of dust in clouds from 25 per cent could be reasonable for some galaxies, in particular, for star forming galaxies at high redshift (e.g. Daddi et al. 2010). The inset of Fig. 11 shows that assuming  $f_{\text{cloud}} = 0.7$  increases the amplitude of the UV luminosity function of LBGs modelled with the SMC extinction law, so it gets closer to the prediction obtained using the MW extinction law and therefore to the observational data. However, the predicted galaxies still populate a similar region in the colour-colour plane shown in Fig. 11 and we find a UV continuum slope consistent with that obtained starting with the default value of  $f_{\text{cloud}} = 0.25$ .

We have tested that changing either  $f_{\text{cloud}}$  or  $t_{\text{esc}}$  has a negligible impact on the predicted UV colours of model

galaxies. However, the luminosity function depends on these parameters and thus, the number of selected LBGs will be different for different sets of parameters. This implies that UV colours cannot constrain the dust parameters,  $f_{\text{cloud}}$  and  $t_{\text{esc}}$ . A similar conclusion was reached by Lo Faro et al. (2009) in their study of model LBGs at  $4 \leq z \leq 6$ .

### 5.3.2 Changing the spatial distribution of dust

The way dust is distributed in a galaxy with respect to stars affects the resulting attenuation and thus, it might affect the predicted UV colours for a given galaxy. By default in GALFORM it is assumed that the scale height of the dust distribution follows exactly that of the stars,  $h_{z,\text{dust}}/h_{z,\text{stars}} = 1$ . In order to explore how this affects the predicted UV colours and luminosity functions of LBGs at  $3 \leq z \leq 8.2$ , we have made predictions for two other cases: when dust is more concentrated than stars,  $h_{z,\text{dust}}/h_{z,\text{stars}} = 0.4$ , and when it is more extended,  $h_{z,\text{dust}}/h_{z,\text{stars}} = 2.5$ .

The UV luminosity function is affected by the change in the relative scale heights of dust and stars. When dust is more concentrated, it affects the light of a smaller fraction of stars and thus the galaxy presents a smaller attenuation compared to the default case of having  $h_{z,\text{dust}}/h_{z,\text{stars}} = 1$ . When the dust has a larger height distribution than the stars, all of the starlight will be affected by dust, as happens in the case of where  $h_{z,\text{dust}}/h_{z,\text{stars}} = 1$ , and thus, the two luminosity functions are very close.

Despite the change in the UV luminosity function, the model galaxies still populate approximately the same region in the UV colour-colour planes.

## 6 THE UV CONTINUUM SLOPE

The rest-frame UV continuum follows approximately a power law,  $f_{\lambda} \propto \lambda^{\beta}$ , and thus, it can be characterised by the slope  $\beta$  (Meurer et al. 1999)<sup>6</sup>. The UV continuum slope is often considered to be directly related to the amount of dust in a galaxy. In Wilkins et al. (2012) we studied the predicted intrinsic (without attenuation) UV continuum slope, measured from a single colour. We found that the distribution of intrinsic UV continuum slopes is affected by the star formation and metal enrichment histories of galaxies and by the choice of the IMF. These dependencies limit the accuracy of the estimation of dust content in galaxies from the observations of UV continuum slopes. We also found that the intrinsic UV continuum slope is correlated with different galaxy properties, including redshift, suggesting that the attenuation by dust inferred from observations may be misestimated, if these trends are not taken into account.

In most observational studies until now the UV continuum slope,  $\beta$ , has been measured from a single UV colour. Although this method is hindered by the photometric errors on the two bands used, a fit to the spectral energy distribution of galaxies at high redshifts is only now becoming possible (Finkelstein et al. 2011; Dunlop et al. 2012). Thus,

<sup>6</sup> Note that a  $\beta = -2$  corresponds to a galaxy with a flat spectrum in terms of  $f_{\nu}$  and, thus a zero UV colour in AB magnitudes.

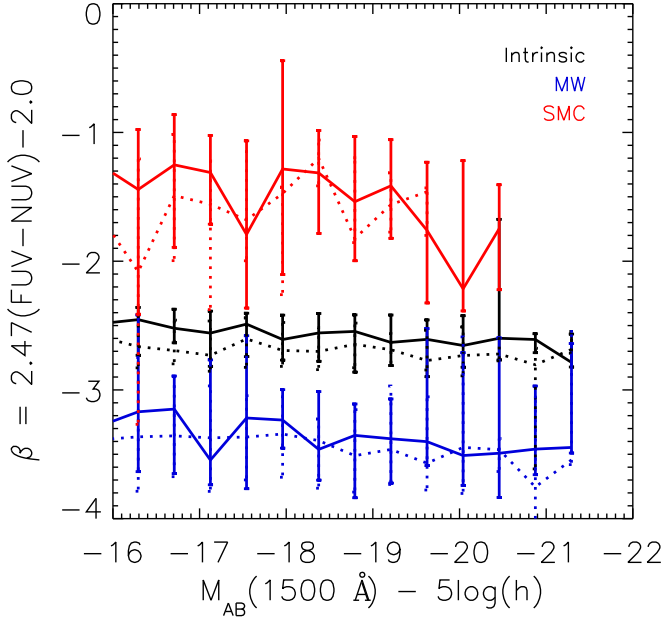


**Figure 12.** The UV continuum slope of model galaxies at  $z = 5$  (solid lines) and  $z = 7$  (dotted lines) measured with two top-hat filters, NUV ( $\sim 1500\text{\AA}$ ) and FUV ( $\sim 2200\text{\AA}$ ), as a function of the rest-frame UV absolute magnitude. The black line corresponds to the intrinsic UV continuum slope and the blue/red to that obtained using the MW/SMC extinction curve as the input for the dust attenuation calculation.

in order to facilitate a comparison with different observational studies, we calculate  $\beta$  using a single UV colour.

We have studied the impact on the UV continuum slope of modifying all the model parameters discussed in §5. We find that the main sensitivity is to the input extinction curve, which we discuss further below. As expected from the previous sections, changing the SPS model does not affect the predicted UV continuum slope. We have previously seen that the IGM attenuation modifies the UV colours, since this effect acts to enhance the strength of Lyman-break. However, the effect that the IGM attenuation has on the UV continuum slope is negligible. We have studied how the UV continuum slope is modified when the scale height of dust is different from that of stars. As we saw in §5.3.2 such a change mainly modifies the UV luminosity function. Accordingly, if no magnitude cut is applied, we find no variation in the UV continuum slope when we go from  $h_{z,dust}/h_{z,stars} = 1$  to  $h_{z,dust}/h_{z,stars} = 0.4$  or to  $h_{z,dust}/h_{z,stars} = 2.5$ , in the studied redshift range. Similar results are found when changing the parameters controlling the fraction of dust in clouds and the migration time out of clouds for young stars.

### 6.1 The change of the UV continuum slope with luminosity

Fig. 12 shows the median UV continuum slope for galaxies at  $z = 5$  and  $z = 7$ . The UV continuum slope,  $\beta$ , has been obtained using:

$$\beta = 2.47(\text{FUV} - \text{NUV}) - 2, \quad (5)$$

where (FUV-NUV) is the rest-frame UV colour calculated with two top hat filters covering the wavelength range:  $1300 \leq \lambda_{\text{FUV}}(\text{\AA}) \leq 1700$  and  $1800 \leq \lambda_{\text{NUV}}(\text{\AA}) \leq 2600$ <sup>7</sup>.

As reported in Wilkins et al. (2012), our galaxy formation model predicts an intrinsic UV continuum slope that is practically independent of the UV luminosity of galaxies. We find that the predicted UV continuum slope varies by less than 0.2 magnitudes for  $-22 \leq M_{\text{UV}} - 5\log h \leq -16$ . We find an intrinsic UV continuum slope of about  $-2.5$  for galaxies  $5 \leq z \leq 7$ . Similar values have been found in hydrodynamical simulations developed to study LBGs at  $z > 5$  (Forero-Romero et al. 2010; Dayal & Ferrara 2012).

Fig. 12 also shows the predicted UV continuum slope once the effect of dust is taken into account, starting from either the MW or the SMC extinction curves. We find that the UV continuum slope is very sensitive to the extinction curve used as input for the dust attenuation calculations. For the chosen set of filters, we find that, as expected, galaxies get redder when the dust attenuation is calculated starting with the SMC extinction curve. However, as shown in Fig. 12 model galaxies get *bluer* when the dust attenuation is calculated starting with the MW extinction curve.

This behaviour is directly related to the  $2175\text{\AA}$  bump in the MW extinction curve shown in Fig. 1, that is still present once the geometry of the dust is taken into account, as seen for the 8 example galaxies in Fig. 10. Thus, this behaviour will depend on the particular set of filters chosen to measure the galaxy colour and it is expected to be reduced if a SED fitting is used to calculate the UV continuum slope. Both Forero-Romero et al. (2010) and Dayal & Ferrara (2012) estimated the UV continuum slope by SED fitting their model galaxies, finding very good agreement with the observed values. These two studies estimated the dust attenuation assuming the simple approximation of a dust slab. Dayal & Ferrara (2012) assumed that the dust present in galaxies at  $z > 6$  is produced solely by Type-II SNe. The extinction curve of dust produced solely by SNe presents a bump at  $\sim 2500\text{\AA}$  and a very steep slope in the UV (Bianchi & Schneider 2007). These characteristics could also imply that galaxies with dust solely produced by SNe will appear to having bluer UV continuum slopes if they were estimated using a single colour.

#### 6.1.1 Comparison with observations

In order to directly test our predictions against observations, we calculate  $\beta$  using the exact filters and equations proposed in different studies that use a single UV colour to estimate the slope of the UV continuum. Fig. 13 shows the predicted intrinsic UV continuum slopes calculated following different observational studies for galaxies at  $z \sim 5, 6$  and  $7$ , using the magnitude and colour cuts summarised in the Appendix.

At  $z = 6$ , Fig. 13 illustrates how, when starting from the MW extinction curve, model galaxies can look redder, the same or even *bluer* than their intrinsic colours, depending on the choice of filters. This is directly related to the  $2175\text{\AA}$  bump being sampled or not by the two chosen filters. This extreme sensitivity of  $\beta$  to the choice of colour used in

<sup>7</sup> Note that these two filters cover the same wavelength range as the GALEX filters.

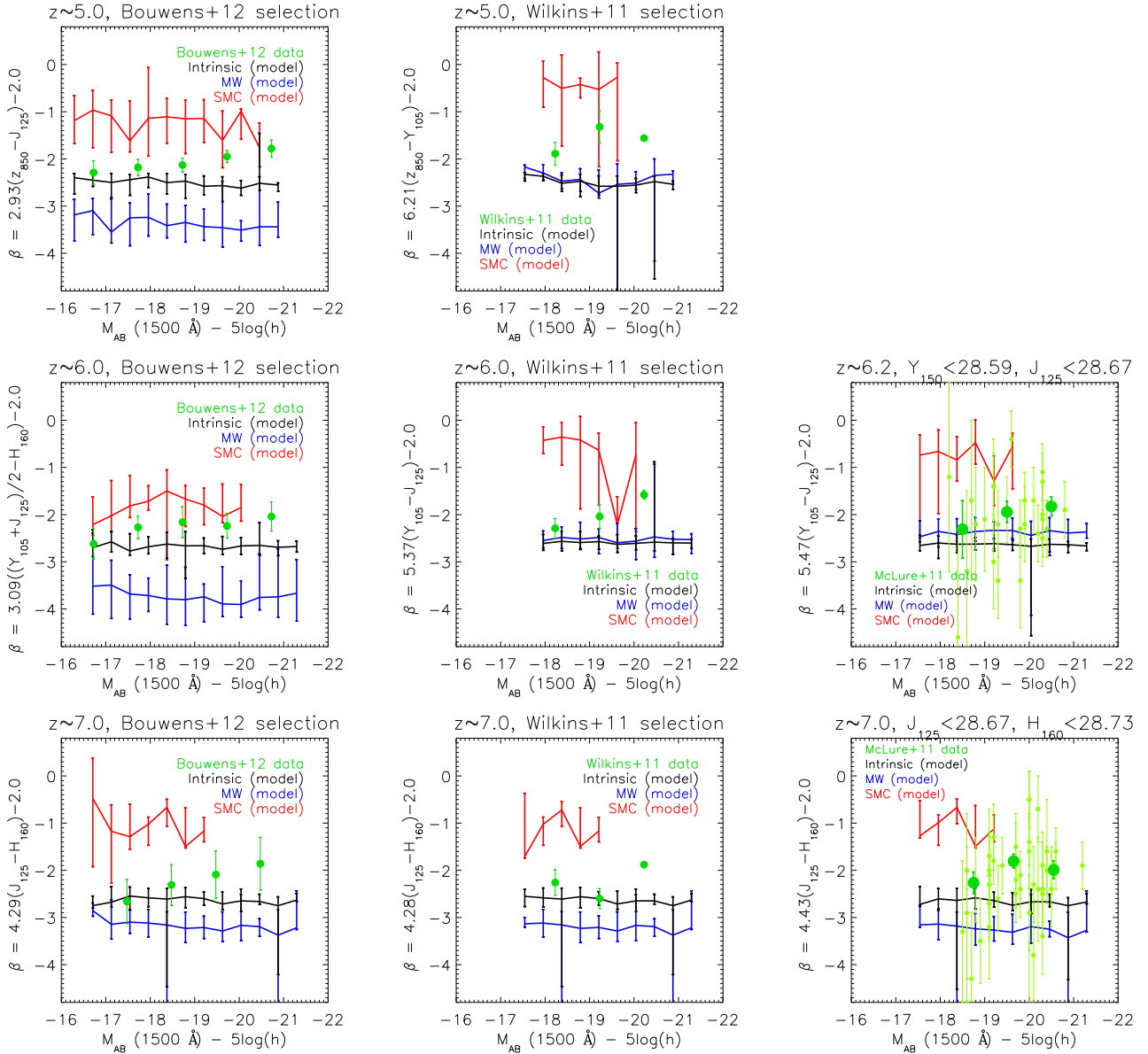


**Figure 13.** The predicted median intrinsic UV continuum slope (black lines) and the attenuated slope, starting either with the MW (blue lines) or the SMC extinction curve (red lines), as a function of absolute attenuated UV magnitude, for galaxies at  $z \sim 5$  (top),  $z \sim 6$  (middle row),  $z \sim 7$  (bottom), selected following the magnitude and colour cuts proposed in different observational studies (summarised in the Appendix). The different columns correspond to the UV continuum slope calculated following the method adopted in the observational studies indicated on the top of each plot. The green circles present, for comparison, the observational data from Bouwens et al. (2012) (left column), Wilkins et al. (2011b) (middle column) and McLure et al. (2011) (right column, who selected LBGs based on photometric redshift and not UV colour cuts). In the latter case we also show the observations for individual galaxies in light green. The mean observational points are shown with their associated errors.

the estimation reinforces the results from Finkelstein et al. (2011), who showed how weakly the UV continuum slope is constrained with a single colour compared with SED fitting using at least 5 bands.

The right column of Fig. 13 shows the UV continuum slopes obtained for individual galaxies in the McLure et al. (2011) sample, together with the mean values per magnitude bin, as shown for the samples from both Bouwens et al. (2012) and Wilkins et al. (2011b) in the other columns of Fig. 13. The scatter when considering individual galaxies is

large enough to cover the UV continuum slopes predicted starting with both the MW and SMC extinction laws. However, McLure et al. (2011) presented a detailed analysis of the problems that affect individual measurements and concluded that averaged UV continuum slopes are more reliable.

Fig. 13 shows that, for some filter combinations, the predicted  $\beta$  including the effect of dust agree with the observations. However, in most cases, the observed mean values are closer to the predicted intrinsic values than to those including the effect of dust.

By doing the exercise of smoothing out the 2175Å bump in the attenuation curves calculated with the Ferrara et al. (1999) model (which are still a function of inclination, optical depth, etc.), we obtain UV continuum slopes about 0.2 magnitudes redder than the intrinsic ones and which are therefore closer to, and in some cases consistent with, the observed values. We have also used the attenuation at 1500Å obtained in the above calculation to normalise the application of the Calzetti law to the model galaxies to derive another illustrative estimate of the attenuation. We find that the attenuation curves from this procedure are greyer than the Calzetti law i.e. there is less wavelength dependence. By using the Calzetti law normalised in this way, we obtain attenuated UV continuum slopes which are consistent with those inferred observationally in at least one magnitude bin at  $z=5, 6$  and 7. Therefore, assuming the Calzetti law, observations are consistent with the predicted 1500Å attenuations.

The predicted values of the UV continuum slope are extremely sensitive to the calculation of the dust attenuation. The observational data are well within the range of predictions when considering either the MW or the SMC extinction curves as input, again emphasising the uncertainty in the treatment of attenuation, and the implications that has when interpreting observational data. It is unclear which extinction curve should be used at different redshifts or even at different luminosities. The fact that the mean observational data have values between the intrinsic model predictions for  $\beta$  and those obtained using the SMC extinction curve, might suggest that the MW extinction curve is not suitable for describing galaxies at  $z \geq 5$ . Nevertheless, the use of the SMC extinction curve appears to be also disfavoured since model galaxies are too red compared with observed ones. Our results suggest that the extinction curve that might describe high redshift galaxies will have characteristics between those of the MW and SMC ones. Conroy et al. (2010) found that the colours of galaxies at  $z < 1$  are best described if it is assumed an attenuation curve with a UV bump strength equal to 80 per cent of that of the MW and a higher effective optical depth in the UV range is assumed, compared with the MW curve.

One clear point of tension in Fig. 13 is the observed trend for  $\beta$  to get bluer for fainter galaxies, something that is not seen in the model galaxies. Nevertheless, Finkelstein et al. (2011) have argued that this trend is in fact due to assuming an average redshift for the whole sample and applying a single correction to estimate  $\beta$  as a function of the rest-frame UV luminosity using fixed filters. Finkelstein et al. found that once a more consistent definition of the rest-frame UV luminosity is used, the trend of the UV continuum slope with UV luminosity disappears. The observations from both Dunlop et al. (2012) and Finkelstein et al. (2011) resulted in mean UV continuum slopes independent of the galaxy luminosity, in agreement with our predictions. These two observational studies selected LBGs by measuring their photometric redshifts and used the galaxy SED to obtain their absolute rest-frame UV magnitude.

For the magnitudes measured in a particular band we do find that brighter galaxies are, on average, more attenuated. However, the model predicts rather grey attenuation and so, the predicted attenuations in the two bands used to compute

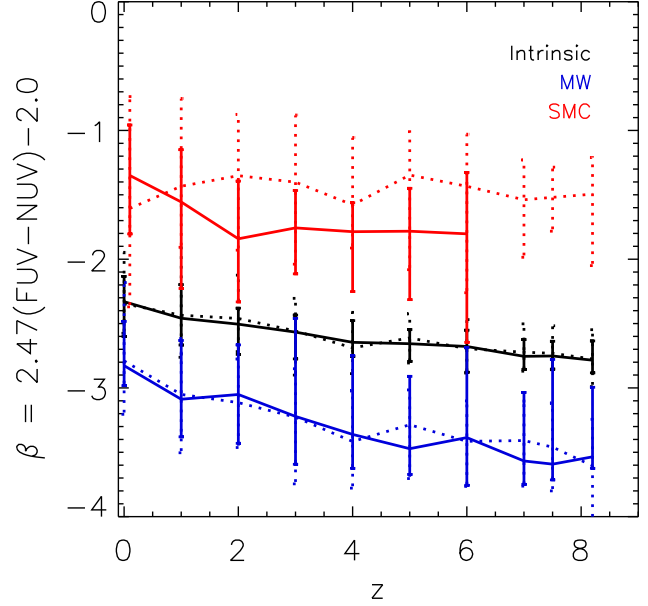


**Figure 14.** The UV continuum slope of galaxies with rest-frame  $M_{UV} - 5\log h \leq -20.3$  (solid lines,  $L_{UV}^*$  at  $z = 3$ ) and  $M_{UV} - 5\log h \leq -17.8$  (dotted lines,  $0.1L_{UV}^*$  at  $z = 3$ ) measured with two rest-frame top-hat filters, NUV ( $\sim 1500\text{\AA}$ ) and FUV ( $\sim 2200\text{\AA}$ ), as a function of redshift. The black line corresponds to the intrinsic UV continuum slope, the blue/red to that obtained using as an input for the model the MW/SMC extinction curve.

$\beta$  are very similar for different HST bands, giving attenuated colours that practically do not depend on the luminosity of a galaxy.

Fig. 13 shows that extracting information about the dust content of a galaxy based on its UV continuum slope could lead to erroneous conclusions if knowledge of the size distribution of dust grains and the galactic inclination is not available.

## 6.2 The change of the UV-continuum slope with redshift.

Fig. 14 shows the evolution with redshift of the intrinsic UV continuum slope, calculated with Eq.5, together with that estimated starting from either a MW or a SMC extinction curve for galaxies with  $M_{AB}(1500\text{\AA}) - 5\log h \leq -20.3$  or  $M_{AB}(1500\text{\AA}) - 5\log h \leq -17.8$ . These two rest-frame magnitudes correspond to  $L_{UV}^*$  and  $0.1L_{UV}^*$  galaxies at  $z = 3$  (Steidel et al. 1999).

The intrinsic UV continuum slope becomes bluer (i.e.  $\beta$  becomes more negative) with increasing redshift. For the intrinsic UV continuum slope, we find a change of 0.5 magnitudes from  $z = 0$  to  $z = 8$ , independently of the absolute magnitude cut. This change is due to an increasing population of young and massive stars at higher redshifts. This result agrees with most observational studies (Bouwens et al. 2009; Finkelstein et al. 2011; Wilkins et al. 2012; Bouwens et al. 2012), but disagrees with the results from Dunlop et al. (2012) for LBGs at  $5 \leq z \leq 7$ . The fact

that the intrinsic UV continuum slope for model galaxies varies with redshift suggests that the trend found observationally may not entirely be driven by the evolution in the dust content of galaxies.

Fig. 14 shows that the effect of using either the SMC or the MW extinction curve impacts the predicted UV continuum slope in a similar way to that reported previously for a fixed redshift. When starting with the MW extinction curve we still find that the UV continuum slope becomes bluer with increasing redshift. However, when starting with the SMC extinction curve the variation of UV continuum slope with redshift is negligible.

## 7 CONCLUSIONS

In this paper we have continued the study started by Lacey et al. (2011) of Lyman-break galaxies (LBG) using GALFORM, the semi-analytical model of galaxy formation originally developed by Cole et al. (2000). We have followed the galaxy formation process in the framework of the  $\Lambda$ CDM cosmology. We have presented predictions for the Baugh et al. (2005) variant of GALFORM, with the same input parameters as those used in Lacey et al. (2011). This model was originally constructed to match the far-UV luminosity function of LBGs only at  $z = 3$  but was shown to fit the observed luminosity functions up to  $z = 10$ , the full range currently available (Lacey et al. 2011).

Here we have studied the predicted rest-frame UV colours of LBGs in the range  $2.5 \leq z \leq 10$ . The Baugh et al. model of galaxy formation includes physical treatments of the hierarchical assembly of dark matter haloes, shock-heating and cooling of gas, star formation, feedback from supernova explosions, the photoionization of the intergalactic medium (IGM), galaxy mergers and chemical enrichment. The luminosities of galaxies are calculated from a stellar population synthesis (SPS) model and dust attenuation is then included using a self-consistent theoretical model based on the results of radiative transfer calculations. The far-UV dust attenuation is a critical component in any model for LBGs, since the effect of dust on UV light can be dramatic.

We find that model galaxies have dust masses that decrease for fainter galaxies. Model galaxies with  $-22 \leq M_{AB}(1500\text{\AA}) - 5\log h \leq -18$  have median dust masses ranging from  $10^{8.5} h^{-1} M_{\odot}$  to  $10^{6.5} h^{-1} M_{\odot}$  at  $z = 3$ . We also find that median dust masses decrease with increasing redshift.

We find that brighter LBGs are generally predicted to be more attenuated at all redshifts than fainter ones, though this trend is dominated by the scatter. Our results suggest that the LBG colour selection does not lead to an appreciable bias in average UV attenuation of the sample.

Our model produces galaxies with UV colours that are generally consistent with the colour-colour region designed observationally for selecting LBGs. From the model results, we expect the drop-out technique to recover most galaxies brighter than the absolute UV magnitude corresponding to the apparent magnitude limit of a particular observational survey. We find the completeness of the drop-out technique to be above 90 per cent at all the studied redshifts, except  $z = 5$ , at which we predict a completeness above 70 per cent. These values should be considered as upper limits, since we have not included the effect of photometric noise,

which most likely will push some galaxies out of the selection region at the target redshift.

We have investigated the impact that different parameters from the model (SPS, IGM and dust treatment) have on the UV colours, finding that they are most sensitive to dust and, in particular, to the extinction curve assumed as an input for the radiative transfer model with which attenuation curves are obtained for individual galaxies. This is related to the fact that the characteristics of the input extinction curves are recognisable in many of the attenuation curves obtained after the processing performed with the radiative transfer model from Ferrara et al. (1999). Nevertheless, we find that the drop-out technique that selects LBGs based on two UV colours is very robust.

The predicted UV luminosity function is strongly affected by changes in the model parameters  $t_{\text{esc}}$ , the time that it takes a star to escape from the molecular cloud in which it is born, and  $f_{\text{cloud}}$ , the fraction of gas and dust in molecular. However, we find that the predicted UV colours are not sensitive to these two parameters. Thus, although the observed UV colours of LBGs are reproduced by the model, the UV colours do not help further to constrain the dust parameters  $t_{\text{esc}}$  and  $f_{\text{cloud}}$ .

We have also obtained the predicted UV continuum slope calculated from a single rest-frame UV colour, as is commonly done in observational studies. For galaxies at redshifts between 5 and 7 we find an intrinsic (without any attenuation) UV continuum slope of about  $-2.5$ , even though some of the brightest galaxies have up to 2 magnitudes of extinction in the UV.

Using the Milky Way (MW) dust extinction curve as an input to the radiative transfer model that calculates dust attenuation, the predicted UV continuum slopes are, in general, *bluer* than observations. However, we find the opposite trend when the Small Magellanic Cloud (SMC) extinction curve is used as an input. This demonstrates the strong dependence of UV colours on dust properties and the inadequacy of using the UV continuum slope as a tracer of dust without further knowledge of the galaxy inclination or dust characteristics. The mean observed UV continuum slopes are close to the predicted intrinsic ones. Including the attenuation by dust produces UV continuum slopes that are either too blue, if assuming a MW extinction curve, or too red, if assuming an SMC extinction curve, compared with the observations. This suggests that neither of these extinction curves provides an adequate description of high redshift galaxies. The discrepancy between the model predictions and the observations for the slope of the attenuated UV continuum slope is smaller than the difference between the predictions obtained using either the MW or SMC extinction curves.

The predicted median UV continuum slope depends very weakly on the rest-frame UV luminosity of galaxies. This result agrees with the observational estimates from both Dunlop et al. (2012) and Finkelstein et al. (2011), but disagrees with other observational studies (Bouwens et al. 2009; Wilkins et al. 2011b; Bouwens et al. 2012). The predicted UV continuum slope gets bluer with increasing redshift, in agreement with many observational studies (Bouwens et al. 2009; Finkelstein et al. 2011; Wilkins et al. 2012; Bouwens et al. 2012), though this trend is not clear when starting with the SMC extinction curve.

In conclusion, we find that the Baugh et al. (2005) model predicts UV colours consistent with the colour-colour regions designed observationally for selecting LBGs. The predicted intrinsic UV continuum slopes are very close to those observed. However, once the (uncertain) dust attenuation is modelled, the predicted and observed UV continuum slope are inconsistent. The discrepancy is extremely sensitive to the choice of input dust extinction curve for the radiative transfer model that calculates the dust attenuation. Actually, it is unclear which dust extinction is appropriate for high redshift galaxies. A better knowledge of dust properties in galaxies at high redshifts will be required to further constrain the models using LBGs.

## ACKNOWLEDGEMENTS

The calculations for this paper were performed on the ICC Cosmology Machine, which is part of the DiRAC Facility jointly funded by STFC, the Large Facilities Capital Fund of BIS, and Durham University. We thank Tom Theuns, Pratika Dayal, Andrea Ferrara, Eli Dwek and the anonymous referee for helpful comments. VGP acknowledges support from the UK Space Agency. VGP, CGL and CMB acknowledge support from the Durham STFC rolling grant in theoretical cosmology.

## REFERENCES

- Baugh C. M., 2006, *Reports of Progress in Physics*, 69, 3101
- Baugh C. M., Cole S., Frenk C. S., Lacey C. G., 1998, *ApJ*, 498, 504
- Baugh C. M., Lacey C. G., Frenk C. S., Granato G. L., Silva L., Bressan A., Benson A. J., Cole S., 2005, *MNRAS*, 356, 1191
- Benson A. J., 2010, *Physics Reports*, 495, 33
- Benson A. J., Bower R. G., Frenk C. S., Lacey C. G., Baugh C. M., Cole S., 2003, *ApJ*, 599, 38
- Benson A. J., Nusser A., Sugiyama N., Lacey C. G., 2001, *MNRAS*, 320, 153
- Bianchi S., Schneider R., 2007, *MNRAS*, 378, 973
- Bouwens R. J. et al., 2009, *ApJ*, 705, 936
- Bouwens R. J., Illingworth G. D., Franx M., Ford H., 2007, *ApJ*, 670, 928
- Bouwens R. J. et al., 2011, *Nature*, 469, 504
- Bouwens R. J. et al., 2012, *ApJ*, 754, 83
- Bouwens R. J. et al., 2003, *ApJ*, 595, 589
- Bressan A., Granato G. L., Silva L., 1998, *A&A*, 332, 135
- Bruzual G., Charlot S., 2003, *MNRAS*, 344, 1000
- Buat V. et al., 2011a, *A&A*, 533, A93
- Buat V., Giovannoli E., Takeuchi T. T., Heinis S., Yuan F.-T., Burgarella D., Noll S., Iglesias-Páramo J., 2011b, *A&A*, 529, A22
- Buat V. et al., 2012, *A&A*, 545, A141
- Burgarella D. et al., 2011, *ApJL*, 734, L12
- Calzetti D., Armus L., Bohlin R. C., Kinney A. L., Koornneef J., Storchi-Bergmann T., 2000, *ApJ*, 533, 682
- Calzetti D., Kinney A. L., Storchi-Bergmann T., 1994, *ApJ*, 429, 582
- Cen R., 2011, *ApJL*, 742, L33
- Chapman S. C., Blain A. W., Smail I., Ivison R. J., 2005, *ApJ*, 622, 772
- Cole S., Lacey C. G., Baugh C. M., Frenk C. S., 2000, *MNRAS*, 319, 168
- Conroy C., Gunn J. E., White M., 2009, *ApJ*, 699, 486
- Conroy C., Schiminovich D., Blanton M. R., 2010, *ApJ*, 718, 184
- Daddi E. et al., 2010, *ApJ*, 713, 686
- Dayal P., Ferrara A., 2012, *MNRAS*, 421, 2568
- Dunlop J. S., 2012, *ArXiv e-prints*
- Dunlop J. S., Hughes D. H., Rawlings S., Eales S. A., Ward M. J., 1994, *Nature*, 370, 347
- Dunlop J. S., McLure R. J., Robertson B. E., Ellis R. S., Stark D. P., Cirasuolo M., de Ravel L., 2012, *MNRAS*, 420, 901
- Dwek E., Cherkneff I., 2011, *ApJ*, 727, 63
- Dwek E., Galliano F., Jones A. P., 2007, *ApJ*, 662, 927
- Ferrara A., Bianchi S., Cimatti A., Giovanardi C., 1999, *ApJS*, 123, 437
- Finkelstein S. L. et al., 2011, *ArXiv e-prints*
- Finlator K., Davé R., Papovich C., Hernquist L., 2006, *ApJ*, 639, 672
- Fioc M., Rocca-Volmerange B., 1997, *A&A*, 326, 950
- Fischera J., Dopita M., 2011, *A&A*, 533, A117
- Fontanot F., Somerville R. S., 2011, *MNRAS*, 416, 2962
- Fontanot F., Somerville R. S., Silva L., Monaco P., Skibba R., 2009, *MNRAS*, 392, 553
- Forero-Romero J. E., Yepes G., Gottlöber S., Knollmann S. R., Khalatyan A., Cuesta A. J., Prada F., 2010, *MNRAS*, 403, L31
- González J. E., Lacey C. G., Baugh C. M., Frenk C. S., 2011, *MNRAS*, 413, 749
- González J. E., Lacey C. G., Baugh C. M., Frenk C. S., Benson A. J., 2012, *MNRAS*, 423, 3709
- Gordon K. D., Clayton G. C., Misselt K. A., Landolt A. U., Wolf M. J., 2003, *ApJ*, 594, 279
- Granato G. L., Lacey C. G., Silva L., Bressan A., Baugh C. M., Cole S., Frenk C. S., 2000, *ApJ*, 542, 710
- Guiderdoni B., Rocca-Volmerange B., 1987, *A&A*, 186, 1
- Guo Q., White S. D. M., 2009, *MNRAS*, 396, 39
- Hathi N. P. et al., 2010, *ApJ*, 720, 1708
- Iliev I. T., Mellema G., Pen U.-L., Merz H., Shapiro P. R., Alvarez M. A., 2006, *MNRAS*, 369, 1625
- Inoue A. K., Iwata I., 2008, *MNRAS*, 387, 1681
- Jaacks J., Choi J.-H., Nagamine K., Thompson R., Varghese S., 2012, *MNRAS*, 420, 1606
- Kennicutt, Jr. R. C., 1983, *ApJ*, 272, 54
- Kim T.-S., Hu E. M., Cowie L. L., Songaila A., 1997, *AJ*, 114, 1
- Kurucz R. L., 1993, *SYNTHES* spectrum synthesis programs and line data, Kurucz, R. L., ed.
- Lacey C. G., Baugh C. M., Frenk C. S., Benson A. J., 2011, *MNRAS*, 45
- Lacey C. G. et al., 2012, *MNRAS*, in prep
- Lacey C. G., Baugh C. M., Frenk C. S., Silva L., Granato G. L., Bressan A., 2008, *MNRAS*, 385, 1155
- Lagos C. D. P., Lacey C. G., Baugh C. M., Bower R. G., Benson A. J., 2011, *MNRAS*, 416, 1566
- Lee K.-S., Alberts S., Atlee D., Dey A., Pope A., Jannuzi B. T., Reddy N., Brown M. J. I., 2012, *ApJL*, 758, L31
- Leisawitz D., Hauser M. G., 1988, *ApJ*, 332, 954
- Lo Faro B., Monaco P., Vanzella E., Fontanot F., Silva L., Cristiani S., 2009, *MNRAS*, 399, 827

- Lorenzoni S., Bunker A. J., Wilkins S. M., Stanway E. R., Jarvis M. J., Caruana J., 2011, MNRAS, 414, 1455
- Madau P., 1995, ApJ, 441, 18
- Madau P., Ferguson H. C., Dickinson M. E., Giavalisco M., Steidel C. C., Fruchter A., 1996, MNRAS, 283, 1388
- Maraston C., 2005, MNRAS, 362, 799
- McLure R. J., Cirasuolo M., Dunlop J. S., Foucaud S., Almaini O., 2009, MNRAS, 395, 2196
- McLure R. J., Dunlop J. S., Cirasuolo M., Koekemoer A. M., Sabbi E., Stark D. P., Targett T. A., Ellis R. S., 2010, MNRAS, 403, 960
- McLure R. J. et al., 2011, MNRAS, 418, 2074
- McMahon R. G., Omont A., Bergeron J., Kreysa E., Haslam C. G. T., 1994, MNRAS, 267, L9
- Meiksin A., 2006, MNRAS, 365, 807
- Meurer G. R., Heckman T. M., Calzetti D., 1999, ApJ, 521, 64
- Michałowski M. J., Murphy E. J., Hjorth J., Watson D., Gall C., Dunlop J. S., 2010, A&A, 522, A15
- Nagamine K., 2002, ApJ, 564, 73
- Nagashima M., Lacey C. G., Okamoto T., Baugh C. M., Frenk C. S., Cole S., 2005, MNRAS, 363, L31
- Noll S. et al., 2009, A&A, 499, 69
- Oesch P. A. et al., 2010, ApJL, 709, L16
- Orsi A., Lacey C. G., Baugh C. M., Infante L., 2008, MNRAS, 391, 1589
- Ouchi M. et al., 2009, ApJ, 706, 1136
- Parkinson H., Cole S., Helly J., 2008, MNRAS, 383, 557
- Raičević M., Theuns T., Lacey C., 2011, MNRAS, 410, 775
- Reddy N. et al., 2012, ApJ, 744, 154
- Reddy N. A., Steidel C. C., 2009, ApJ, 692, 778
- Robertson B. E., Ellis R. S., Dunlop J. S., McLure R. J., Stark D. P., 2010, Nature, 468, 49
- Robson I., Priddey R. S., Isaak K. G., McMahon R. G., 2004, MNRAS, 351, L29
- Sawicki M., Thompson D., 2006, ApJ, 642, 653
- Schroeder J., Mesinger A., Haiman Z., 2012, ArXiv e-prints
- Shimasaku K., Ouchi M., Furusawa H., Yoshida M., Kashikawa N., Okamura S., 2005, PASJ, 57, 447
- Silva L., Granato G. L., Bressan A., Danese L., 1998, ApJ, 509, 103
- Somerville R. S., Gilmore R. C., Primack J. R., Domínguez A., 2012, MNRAS, 423, 1992
- Steidel C. C., Adelberger K. L., Giavalisco M., Dickinson M., Pettini M., 1999, ApJ, 519, 1
- Steidel C. C., Giavalisco M., Dickinson M., Adelberger K. L., 1996, AJ, 112, 352
- Steidel C. C., Hamilton D., 1992, AJ, 104, 941
- Steidel C. C., Pettini M., Hamilton D., 1995, AJ, 110, 2519
- Valiante R., Schneider R., Bianchi S., Andersen A. C., 2009, MNRAS, 397, 1661
- Valiante R., Schneider R., Salvadori S., Bianchi S., 2011, MNRAS, 416, 1916
- Vijh U. P., Witt A. N., Gordon K. D., 2003, ApJ, 587, 533
- Wild V., Charlot S., Brinchmann J., Heckman T., Vince O., Pacifici C., Chevallard J., 2011, MNRAS, 417, 1760
- Wilkins S. M., Bunker A. J., Lorenzoni S., Caruana J., 2011a, MNRAS, 411, 23
- Wilkins S. M., Bunker A. J., Stanway E., Lorenzoni S., Caruana J., 2011b, MNRAS, 417, 717
- Wilkins S. M. et al., 2012, submitted to MNRAS
- Yan H.-J., Windhorst R. A., Hathi N. P., Cohen S. H., Ryan R. E., O'Connell R. W., McCarthy P. J., 2010, Research in Astronomy and Astrophysics, 10, 867
- Yoshida M. et al., 2006, ApJ, 653, 988
- Zafar T., Watson D. J., Malesani D., Vreeswijk P. M., Fynbo J. P. U., Hjorth J., Levan A. J., Michałowski M. J., 2010, A&A, 515, A94

## APPENDIX

Here we define explicitly the magnitude and colour cuts used to select the model LBGs at different redshifts. The magnitude cuts have been chosen to be either the magnitude cutoff used in the observational studies to define their LBGs sample or the  $3\sigma$  (or  $5\sigma$ ) detection limits quoted in those studies for the bands sampling the UV continuum slope in the deepest field of the study.

- **U-dropouts**,  $3 \leq z \leq 3.5$ , **Steidel et al. (1995) selection:**  $\mathcal{R} < 25.5$  and  $G < 27.3$  and  $(U_n - G) > 1.5$  and  $(U_n - G) > (G - \mathcal{R}) + 1.5$  and  $(G - \mathcal{R}) < 1.2$  and  $(G - \mathcal{R}) > 0$

- **B-dropouts**,  $z \sim 4$ , **Bouwens et al. (2012) selection:**  $V_{606} < 30.1$  and  $z_{850} < 29.4$  and  $(V_{606} - z_{850}) < 1.6$  and  $(B_{435} - V_{606}) > 1.1$  and  $(B_{435} - V_{606}) > (V_{606} - z_{850}) + 1.1$

- **V-dropouts**,  $z \sim 5$ , **Bouwens et al. (2012) selection:**  $i_{775} < 29.9$  and  $z_{850} < 29.4$  and  $[(V_{606} - i_{775}) > (i_{775} - z_{650}) + 1.5$  or  $(V_{606} - i_{775}) > 2]$  and  $(i_{775} - z_{650}) < 0.8$

- **V-dropouts**,  $z \sim 5$ , **Wilkins et al. (2011b) selection:**  $z_{850} < 27.9$  and  $(z_{850} - Y_{105}) < 0.62$  and  $(V_{606} - i_{775}) > 0.81(z_{850} - Y_{105}) + 2.14$  and  $(i_{775} - z_{850}) < 0.76(z_{850} - Y_{105}) + 0.83$

- **i-dropouts**,  $z \sim 6$ , **Bouwens et al. (2012) selection:**  $z_{850} < 29.4$  and  $J_{125} < 29.9$  and  $(i_{775} - z_{850}) > 1.3$  and  $(z_{850} - J_{125}) < 0.9$

- **i-dropouts**,  $z \sim 6$ , **Wilkins et al. (2011b) selection:**  $Y_{105} < 28.1$  and  $(Y_{105} - J_{125}) < 0.78$  and  $(i_{775} - z_{850}) > 0.56(Y_{105} - J_{125}) + 1.27$  and  $(z_{850} - Y_{105}) < 0.66(Y_{105} - J_{125}) + 0.73$

- **z-dropouts**,  $z \sim 7$ , **Bouwens et al. (2012) selection:**  $Y_{105} < 29.6$  and  $J_{125} < 29.9$  and  $(z_{850} - Y_{105}) > 0.7$  and  $(Y_{105} - J_{125}) < 0.8$  and  $(z_{850} - Y_{105}) > 1.4(Y_{105} - J_{125}) + 0.42$

- **z-dropouts**,  $z \sim 7$ , **Wilkins et al. (2011b) selection:**  $J_{125} < 28.5$  and  $(J_{125} - H_{160}) < 0.95$  and  $(Y_{105} - J_{125}) < 0.46(J_{125} - H_{160}) + 0.89$  and  $(z_{850} - Y_{105}) > 0.42(J_{125} - H_{160}) + 1.48$

- **Y-dropouts**,  $z \sim 8$ , **Lorenzoni et al. (2011) selection:**  $J_{125} < 28.5$  and  $(Y_{105} - J_{125}) > 0.9$  and  $(J_{125} - H_{160}) < 1.5$  and

$$(Y_{105} - J_{125}) > 0.73(J_{125} - H_{160}) + 0.9$$

• **J-dropouts**,  $z \sim 10$ , **Bouwens et al. (2011) selection**:  $H_{160} < 29.8$  and  $(J_{125} - H_{160}) > 1.2$